KIEL Institut

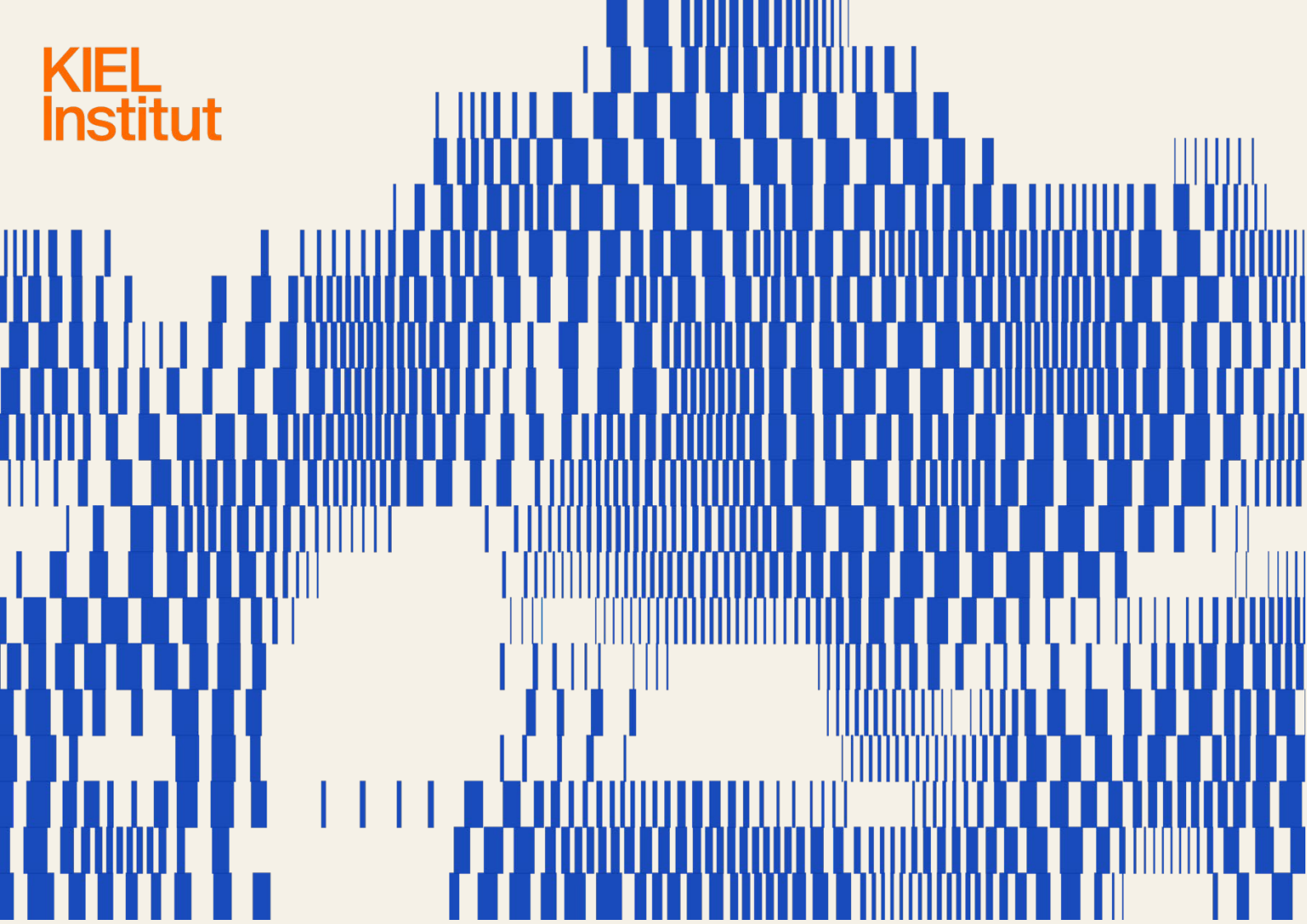

Felix Meier, Martin Quaas, Wilfried Rickels,
Christian Traeger

January 2026

From Gross to Net: Carbon Dioxide Removal in an Analytic Climate Economy

Kiel Working Paper

No. 2313, ISSN 1862-1155
Kiel Institute for the World Economy

Abstract*

Felix Meier, Martin Quaas, Wilfried Rickels, Christian Traeger #

Carbon dioxide removal (CDR) is considered essential for climate change mitigation, yet its optimal role in climate policy remains unclear in the presence of non-permanent storage, energy constraints, and fossil fuel scarcity. We integrate CDR into an analytic integrated assessment model to derive general conditions for socially optimal CDR deployment. Within a linear carbon cycle model, we consider different CDR pathways, including direct air carbon capture, ocean alkalinity enhancement, and ocean iron fertilization. Introducing CDR does not significantly alter the optimal carbon price and the incentive to reduce emissions. The impact of CDR on gross emissions mainly stems from the energy required to operate it. This impact, as well as the optimal deployment of CDR, depends on fossil fuel scarcity and the pace of renewable energy deployment. In high-damage scenarios, the optimal deployment of CDR occurs before and around the year 2100, consistent with temperature overshoot pathways.

Keywords: carbon dioxide removal, climate change, integrated assessment, social cost of carbon
JELs: Q54

Authors

Felix Meier
Kiel Institute for the World Economy
felix.meier@kielinstitut.de
www.kielinstitut.de

Martin Quaas
German Centre for Integrative Biodiversity Research (iDiv) Halle-Jena-Leipzig
martin.quaas@idiv.de
www.idiv.de

Wilfried Rickels
Kiel Institute for the World Economy
wilfried.rickels@kielinstitut.de
www.kielinstitut.de

Christian Traeger
University of Oslo & ifo Institute for Economic Research
traeger@uio.no
www.uio.no

*This paper supersedes the earlier version titled "Carbon dioxide removal in a global analytical climate economy" released in 2022

#We are grateful for feedback on earlier drafts from the audiences at EAERE 2022 & SURED 2022 and the seminar participants at PIK 2022. We also thank three anonymous reviewers and the editor for their very helpful comments. E-mail addresses: felix.meier@kielinstitut.de (F.M.), martin.quaas@idiv.de (M.Q.), wilfried.rickels@kielinstitut.de (W.R.), traeger@uio.no (C.T.). F.M. and C.T. acknowledge funding from the European Union's Horizon 2020 research and innovation programme under grant agreement No 869357 (OceanNETs). F.M. acknowledges funding by the German Research Foundation (DFG, RI 1833/4-1). W.R. acknowledges funding from the Volkswagen AG as part of an endowed professorship via the Stifterverband.

1 Introduction

Meeting the temperature goals of the Paris Agreement requires rapid reductions in anthropogenic CO_2 emissions and atmospheric removal of CO_2 (Babiker et al. 2022). Carbon dioxide removal (CDR) can offset expensive-to-abate emissions and, in overshoot pathways, help return atmospheric CO_2 concentrations to lower levels. CDR covers a wide set of approaches that increase or complement natural sequestration, ranging from land-based measures to engineered options such as direct air capture (Klepper and Rickels 2014; Fridahl et al. 2023; Edenhofer et al. 2025).

At the same time, CDR is not a frictionless backstop. Most options are energy and resource intensive, so deployment can raise gross energy demand and, when that energy is carbon intensive, gross emissions. Moreover, the climate benefit of removing one ton of CO_2 depends on where the carbon is stored and how durable that storage is. Storage in reservoirs that exchange carbon with the atmosphere, or that leak over time, yields a smaller long-run benefit than effectively permanent storage. These features complicate both welfare assessment and the design of price-based climate policy. A central policy question is therefore how to integrate CDR into carbon pricing and trading systems. Treating verified removals as negative emissions can improve efficiency (e.g. Galán-Martín et al. 2021; Rickels et al. 2022; Edenhofer et al. 2023), but it has also raised concerns about delayed structural changes in decarbonization (e.g., Geden et al. 2019; Anderson et al. 2023; Brad and Schneider 2025) and about the appropriate valuation of temporary storage (Herzog et al. 2003; Groom and Venmans 2023).

This paper studies these issues by identifying the key drivers that govern the role of CDR in welfare-optimizing climate policy. We do so using a transparent analytical integrated assessment model that embeds CDR in a macroeconomic growth framework with an explicit multi-reservoir carbon cycle and an energy system in which removal competes with other uses of energy and interacts with fossil fuel scarcity and the transition to renewables. The analytical structure delivers closed-form conditions that clarify (i) how the social value of CDR is governed by the wedge between the shadow value of carbon in the source reservoir and in the storage reservoir, a wedge that shrinks with leakage and other return flows, (ii) how CDR affects gross and net emissions through its energy requirements and through general-equilibrium feedbacks in energy markets, and (iii) how these mechanisms translate into optimal carbon pricing. A key implication is that the atmospheric social cost of carbon (SCC),[1] which determines the optimal carbon tax along the optimal path, is nearly unchanged by the availability of CDR. Hence, the marginal incentive to abate emissions via the carbon price remains largely intact, and any increase in gross emissions operates primarily through an increase in energy demand rather than

1. Throughout the paper, we use the term SCC to denote the social cost of atmospheric carbon, as opposed to the social cost of carbon stored in other reservoirs (e.g., the ocean reservoir), which we distinguish explicitly where relevant.

through a lower carbon price. However, because fossil energy is exhaustible, higher energy demand raises the Hotelling scarcity rent; by the Hotelling rule this discourages current extraction and lowers current emissions, thereby dampening the gross-emissions response to CDR.

We complement the theory with a calibrated quantitative analysis for three prominent CDR pathways (direct air capture with carbon storage, ocean alkalinity enhancement, and ocean iron fertilization) and for carbon capture and storage (CCS). The quantitative results highlight how differences in removal pathways and storage dynamics translate into distinct optimal timing and scale. In particular, approaches differ in when they enter and how fast they scale as costs fall, as the energy system decarbonizes, and as the scarcity of fossil inputs changes. They also quantify the central role of storage durability: even modest departures from permanent storage can sharply reduce the optimal scale of DACCS-like options, while ocean-based approaches are inherently constrained by the inertia of ocean uptake and mixing. Across damage and technology scenarios, CDR primarily reshapes optimal mitigation from gross to net carbon accounting, enabling net-zero and temporary net-negative emissions and therefore overshoot dynamics, with removals concentrated before and around 2100 in high-damage cases. Finally, the simulations illustrate that the energy requirements of large-scale CDR and CCS can become quantitatively important, so the pace of the clean energy transition and the degree of fossil scarcity are first-order determinants of optimal deployment.

A fundamental concern regarding the integration of CDR in climate policy arises from the possibility of substituting emissions reductions (Brad and Schneider 2025). Accordingly, proposals are being discussed to retain CDR as a separate pillar of climate policy so that the price within emissions trading does not fall and the incentives for emissions reductions remain unchanged (Anderson and Newell 2004). Kalkuhl et al. (2022) use a dynamic partial equilibrium model without fossil fuel resource scarcity and find that CDR could decrease the carbon price by up to 10% by 2100 (as displayed in their Figure 6), leading to an increase in the use of fossil energy. We consider instead a macroeconomic growth model, building on the recently developed analytic IAMs (Golosov et al. 2014; Gerlagh and Liski 2018; Traeger 2023), which specify utility and climate damage functions such that the climate-economy model becomes linear in the model's state variables (Karp 2017; Traeger 2023). Given the linear-in-states property of the analytic IAM, we show that the deployment of CDR technologies has no direct effect on the analytic structure of the SCC. However, CDR does influence the time path of total economic output, thus impacting the level of the SCC. This effect, however, is only of second-order relevance, and may go either way. Accordingly, we show that the optimal carbon tax, which is equivalent to the SCC at the optimal path, is nearly unaffected by the availability of CDR methods. Consequently, the incentives for abating CO_2 emissions via the carbon price remain largely unaffected when including CDR in climate policy. Or to put it dif-

ferently, the marginal benefit of emission abatement is largely unaffected by CDR. This result is specific to CDR and sets it apart from Solar Radiation Management, which can lead to a substantial reduction in the SCC and therefore emissions reductions (Meier and Traeger 2022).

However, the implications of CDR deployment for gross emissions are determined not only by the interaction with the carbon tax but also by interaction with energy consumption. Studies suggest that novel CDR like direct air carbon capture and storage (DACCS) require substantial energy input. For example, Realmonte et al. (2019) show that a large-scale implementation of direct air capture would require 10% to 15% of annual global energy provision by 2100. However, as of 2022, modern renewable energy sources, excluding traditional uses of biomass, accounted for only 13% of global final energy consumption (International Energy Agency 2025). To account for the energy intensiveness of CDR, we measure the operational cost of CDR in energy equivalents and show how the increasing share of renewable energy provision affects CDR deployment levels. Kalkuhl et al. (2022) assume perfect substitutability between fossil and renewable inputs. We allow for limited substitutability, as some important sectors, like aviation or the production of steel and cement, are hard to decarbonize. Additionally, our model diverges from Kalkuhl et al. (2022)'s assumption that the supply of fossil inputs is unlimited. We show that neglecting the increasing scarcity of fossil resources and the limited substitutability between energy inputs leads to an overestimation of CDR deployment paths. On the other hand we also show how under a high damage function, calibrated against the estimates of Howard and Sterner (2017), the fossil resource stock becomes abundant for climate policies without CDR and CCS and that in this case a notable increase in gross emissions can be observed by the inclusion of CDR. Nevertheless, the impact on net emissions is clear; otherwise, CDR would not be beneficial. In our quantitative analysis, we show that the use of CDR would result in temperature overshoot scenarios in which, in the event of high climate damage and optimistic developments in the costs of CDR and CCS, the peak temperature would already be reached in 2043. By contrast, climate policies without CDR would only result in a smoothing of temperature increase (on timescales up to the year 2200).

Still, a fundamental concern remains regarding the climate change mitigation benefit of CDR in case of non-permanent carbon storage (e.g., Herzog et al. 2003; Sierra et al. 2021; Groom and Venmans 2023). Non-permanent carbon storage might result from leaky geological reservoirs (e.g., Zwaan and Gerlagh 2009) or when carbon is stored in terrestrial or ocean reservoirs interacting with the atmospheric carbon reservoir through natural processes (e.g., Brander et al. 2021; Parisa et al. 2022). Various carbon accounting methods have been proposed and analyzed to assess the climate benefit in the case of non-permanent carbon storage (Brandão et al. 2019; Galik et al. 2022), whereas their practicular appropriateness to organize for example carbon credits issuance requires to

consider the region-specific climate policy and therefore liability framework. On a more general level, Rickels and Lontzek (2012) find that each ton of carbon sequestered in the ocean is optimally taxed at a lower rate than atmospheric carbon emissions, with the benefit of ocean CDR arising from the difference between the two shadow prices corresponding to the atmospheric and oceanic carbon stock. Groom and Venmans (2023) consider non-permanent storage independently of the storage reservoir and derive a general formula for the shadow price of this storage (social value of offset), which measures the value relative to the SCC which in case of permanent storage obviously coincides with the SCC. Our model explicitly allows for different carbon storage pathways. We extend the findings of Rickels and Lontzek (2012) to a growth framework and incorporate the carbon cycle model with an arbitrary number of carbon reservoirs from Traeger (2023) into our analytic IAM. We confirm that the primary driver of CDR is the (relative) difference between the SCC in the atmosphere and in a given storage reservoir. We show that this difference declines sharply in the leakage rate of the storage reservoir. We express this core driver and the various factors influencing CDR deployment through simple formulas and quantify their respective contributions to determining the overall level of CDR. In our quantitative analysis, we apply a three-box carbon cycle model, using the recent calibration from Folini et al. (2025) and consider storage pathways representing DACCS, ocean alkalinity enhancement, and ocean iron fertilization. In addition, we also consider CCS which has in our model the same carbon storage pathway as DACCS, however, restricted to the level of (point-source) emissions and represented by a different cost function.

The paper is structured as follows. Section 2 introduces carbon dioxide removal into a standard analytical climate economy model. Sections 3.1 through 3.3 present the theoretical results on the SCC, optimal CDR deployment, and the implications for emissions and energy use. Section 3.4 extends the baseline model, which features only fossil energy, by introducing renewable energy. This extended model is used for the quantitative analysis. Section 4 calibrates the model for three types of CDR, Direct Air Capture and Carbon Storage (DACCS), Ocean Alkalinity Enhancement (OAE), and Ocean Iron Fertilization (OIF), as well as for a point source abatement technology, Carbon Capture and Storage (CCS). Section 5 presents results for alternative CDR cost scenarios and examines the sensitivity of the findings to assumptions about climate damages, the carbon cycle, and fossil fuel scarcity. Section 6 concludes.

2 Analytic climate-economy model

The analytic integrated assessment model builds on Golosov et al. (2014) and Traeger (2023). We consider a global economy where gross output Y_t at time t is a function of

technology A_t, capital K_t, labor N_t, and energy input I_t,

$$Y_t = A_t \, K_t^{\kappa} \, N_t^{1-\kappa-v} \, I_t^{v}, \tag{1}$$

with given initial capital stock $K_0 > 0$ and parameters $\kappa > 0$, $v > 0$ and $1 - \kappa - v > 0$. Technology and labor are prescribed by exogenous processes, as in the DICE model (Barrage and Nordhaus 2023).

We extend the basic model by distinguishing between net energy usage, I_t, used in production, and gross energy usage, E_t, which also accounts for energy used in CDR deployment. Gross energy usage entails output costs, represented by a cost coefficient γ_t that maps energy use into a proportional reduction in output. Net output is thus given by $Y_t \exp(-\gamma_t E_t)$. This specification captures a central trade-off in CDR deployment between current output losses from energy use and future benefits from lower atmospheric carbon concentrations and, thus, damages.

In the basic model specification, gross energy E_t is extracted from a stock of exhaustible fossil resource R_t, which evolves according to

$$R_{t+1} = R_t - E_t, \qquad \text{with } R_0 > 0 \text{ given.} \tag{2}$$

We think of R_t as an aggregate of coal, oil, and gas, and measure energy in carbon equivalents (in GtC; as in Golosov et al. 2014). In Section 3.4 we additionally consider renewable energy sources.

Together with exogenous emissions from land-use changes, E_t^{exo}, CO_2 from fossil fuel combustion, E_t, net of any point-source carbon capture (CCS), constitutes anthropogenic carbon emissions into the atmosphere. The stock of carbon in the atmosphere, $M_{1,t}$, additionally depends on net carbon flows from and to other reservoirs with stocks $M_{2,t}, \ldots, M_{r,t}$.

As in Traeger (2023), we allow for an arbitrary finite number $r > 1$ of carbon reservoirs ("boxes"), which represents the carbon stocks of different layers of the ocean and the biosphere, and potential geological storage capacities. The changes of carbon stocks in the boxes are described by the linear carbon cycle model

$$\begin{pmatrix} M_{1,t+1} \\ M_{2,t+1} \\ \vdots \\ M_{r,t+1} \end{pmatrix} = \begin{pmatrix} \phi_{11} & \ldots & \phi_{1r} \\ \phi_{21} & \ldots & \phi_{2r} \\ \vdots & \ddots & \vdots \\ \phi_{r1} & \ldots & \phi_{rr} \end{pmatrix} \begin{pmatrix} M_{1,t} \\ M_{2,t} \\ \vdots \\ M_{r,t} \end{pmatrix} + \begin{pmatrix} E_t^{net} + E_t^{\text{exo}} \\ \sum_{j=1}^{r} G_{2,j,t} \\ \vdots \\ \sum_{j=1}^{r} G_{r,j,t} \end{pmatrix}. \tag{3}$$

or, in matrix notation

$$\boldsymbol{M}_{t+1} = \boldsymbol{\Phi} \boldsymbol{M}_t + \boldsymbol{E_t}, \tag{4}$$

where the transition matrix $\mathbf{\Phi}$ characterizes the carbon flows between the reservoirs.

Extending Traeger (2023), we model CDR by allowing for induced carbon transfers $G_{i,j,t}$ from any reservoir $j = 1, \ldots, r$ into any non-atmospheric boxes $i = 2, \ldots, r$ with $i \neq j$. Carbon transfers resulting in a reduction of the carbon stock M_1 classify as atmospheric CDR. Mass balance imposes $G_{i,j,t} = -G_{j,i,t}$.

With the CDR from the atmosphere to other reservoirs, combustion-based net emissions into the atmosphere are

$$E_t^{net} = E_t - \sum_{i=2}^{r} G_{i,1,t}. \tag{5}$$

Accordingly, net emissions can be positive or negative. Direct air carbon capture and storage (DACCS), for example, removes carbon from the atmosphere and stores this amount of carbon in another reservoir i. The model can also include point-source CCS, for which the amount of carbon capture can not exceed gross emissions, E_t. For how long the carbon is removed from the atmosphere depends on the transition rates of carbon between the storage reservoirs. Although we do not consider direct capacity constraints for storage in any of the boxes,[2], a relatively higher amount of carbon in any of the reservoirs increases the carbon fluxes to other reservoirs. If carbon is stored in a geological reservoir, we track the reservoir as part of an extended carbon cycle to incorporate geological carbon leakage. The model also allows for more complicated CDR pathways, such as OIF, which transfers carbon from a non-atmospheric reservoir (e.g., the upper ocean) to another non-atmospheric reservoir (e.g., the deep ocean).

Any carbon transfer $G_{i,j,t}$ is costly, i.e. requiring a positive amount of energy input, which carries opportunity costs in terms of foregone final output. We use $f_{i,j}(G_{i,j,t}) \geq 0$ to denote the amount of energy required for a carbon transfer $G_{i,j,t} > 0$ from j to i. Marginal energy use is positive and increasing for all storage units, $f'_{i,j}(G_{i,j,t}) > 0$ and $f''_{i,j}(G_{i,j,t}) > 0$. We measure the energy costs at the carbon sink, such that without a positive carbon transfer, corresponding costs of CDR are zero, $f_{i,j}(G_{i,j,t}) = 0$ for $G_{i,j,t} = 0$.

Given gross energy E_t, the net energy for input into production is

$$I_t = E_t - \sum_{i=2}^{r} \sum_{j=1}^{r} f_{i,j}(G_{i,j,t}). \tag{6}$$

Thus, CDR reduces final output, reflecting the trade-offs involved in the CDR deployment decision (Renforth et al. 2013; Realmonte et al. 2019). As a reduction of atmospheric carbon can be achieved either by reducing energy input or by CDR, a reservoir i will only be used for CDR if its cost (and marginal cost) is lower than the cost (and marginal cost) of emissions abatement, thus optimality of CDR deployment implies $f_{i,j}(G^*_{i,j,t}) \leq G^*_{i,j,t}$.

2. For a discussion of geological storage constraints see, e.g., Lafforgue et al. (2008) or Hoel (2025)

If no CDR would be used at all, for whatever reason, net energy input, emissions, and net emissions are all the same, $I_t = E_t = E_t^{net}$.

As in Golosov et al. (2014), climate change damage is a function of the atmospheric carbon stock $M_{1,t}$. Climate damage, expressed as a fraction of gross output, is specified as

$$D_t(M_{1,t}) = 1 - \exp\left[-\xi_0 \left(M_{1,t} - M_1^{pre}\right)\right], \tag{7}$$

where M_1^{pre} denotes the pre-industrial atmospheric carbon concentration. The climate change damage parameter $\xi_0 > 0$ scales the marginal climate damage of atmospheric carbon.

Including both climate damage and energy cost, net output is

$$Y_t^{net} = Y_t \left[1 - D_t\left(M_{1,t}\right)\right] \exp(-\gamma_t E_t). \tag{8}$$

As Golosov et al. (2014), capital fully depreciates within one time step (10 years in our calibration). Thus, the economy's capital stock in the next period is given as the difference between net output Y_t^{net}, and consumption C_t,

$$K_{t+1} = Y_t^{net} - C_t \tag{9}$$

We use $x_t = \frac{C_t}{Y_t^{net}}$ to denote the consumption rate, such that $1 - x_t$ is the savings rate.

We solve the model for a social planner who maximizes the present value, with utility discount factor β, of welfare from an infinite stream of consumption flows,

$$\max_{x_t, E_t, \{G_{i,j,t}\}} \sum_{t=0}^{\infty} \beta^t \, \log(c_t), \tag{10}$$

by choosing the consumption rate, emissions, and CDR with storage in reservoir i, subject to the constraints imposed by the economy and the climate system, equations (1) to (9).

3 Theoretical analysis

The advantage of the analytic integrated assessment model is that the trade-offs involved in optimal climate policy and therefore optimal CDR use as well as the relationship between CDR use and the SCC can be characterized explicitly. Here, we first present these results for the base version of the model with only fossil energy sources, and then additional consider the fossil-renewable energy mix in Section 3.4.

As standard in this class of models, the consumption rate is constant, $x_t^* = 1 - \beta\,\kappa$. A high discount factor β, or a high capital share in production κ, both decrease the

consumption rate and increase the savings rate. Energy use diminishes the stock of fossil resources, and thus increases the shadow price of the remaining resource stock. In welfare terms, the shadow price increases exponentially $\varphi_{R,t} = \beta^{-t}\varphi_{R,0}$. Measured in units of the final output good, the shadow price of the resource stock increases at the consumption discount rate (Traeger 2021; see Appendix A for the derivation).

3.1 Social costs of carbon in the different reservoirs

The SCC, as usually considered, is the shadow price of atmospheric carbon, i.e. the present value of marginal climate damages caused by an extra ton of atmospheric carbon, expressed in units of the final output good. Considering the possibility of removing carbon from the atmosphere and storing it in another reservoir, the shadow prices of carbon in these other reservoirs matter as well. We find that the social cost of carbon in reservoir i is given by the formula

$$SCC_{Mi} = Y_t^{net}\,\xi_0\,\left[(\mathbf{1} - \beta\,\mathbf{\Phi})^{-1}\right]_{1,i}, \tag{11}$$

where the subscript $1, i$ indicates the ith element in the first row of the matrix $(\mathbf{1}-\beta\,\mathbf{\Phi})^{-1}$ (see Appendix E). The SCC, in any reservoir, are proportional to (net) output and the damage semi-elasticity ξ_0, as it is the case for the atmospheric SCC in Golosov et al. (2014). The SCC grow with world output. Nordhaus called this increase of the SCC the "climate policy ramp". We find a similar ramp for the SCC not only in the atmosphere, but in all other carbon reservoirs as well.

The difference between the atmospheric SCC and another reservoir's SCC is determined by the last term in equation (11), the carbon dynamics multiplier. It captures the discounted sum of future carbon remaining in, or flowing into, the atmosphere (reservoir 1) resulting from a ton of carbon currently stored in reservoir i, and can be written as (Traeger 2023)[3]

$$\left[(\mathbf{1} - \beta\mathbf{\Phi})^{-1}\right]_{1,i} = \left[\sum_{i=0}^{\infty} \beta^i \mathbf{\Phi}^i\right]_{1,i}. \tag{12}$$

The transition matrix $\mathbf{\Phi}$ accounts for the different diffusion (or leakage) rates across reservoirs, and it's i^{th} power reflects the number of (periodic) transitions. For example, the shallow ocean has a strong exchange with the atmosphere (stronger transition contribution), resulting in a SCC that is relatively close to the atmospheric SCC. By contrast, the deep ocean interacts only very slowly (very small transition contribution), hence the SCC of the deep ocean is much smaller than the atmospheric SCC.

3. $\left[\mathbf{\Phi}^1\right]_{1,i}$ characterizes the fraction of carbon that travels from reservoir i to the atmosphere within one period, in our case 10 years.

The atmospheric SCC, SCC_{M1}, is equivalent to the optimal tax on carbon emitted into the atmosphere (reservoir 1). Similarly, SCC_{M2} would be the socially optimal tax on carbon stored in reservoir 2, for example the upper ocean or biosphere. Ordering the three natural reservoirs like in the DICE carbon cycle as atmosphere, upper ocean, and deep ocean leads to the ranking $SCC_{M1} > SCC_{M2} > SCC_{M3}$. The SCC for geological reservoirs depends on the geological leakage rate into the atmosphere. Only a geological storage with zero leakage, i.e., a reservoir not in direct or indirect exchange (via other reservoirs) with the atmosphere would have a SCC of zero: carbon from such a reservoir never reaches the atmosphere and never causes climate damage.

An important aspect of the result (11) is that the optimal carbon taxes for the different reservoirs are independent of the carbon stocks (except for Y_t^{net} 's direct dependence on damages). Thus, they are also independent of he amount of CDR deployed. This reflects that the marginal damage of carbon is constant, which comes about as the convexity of damages in temperature approximately offsets the concavity of the greenhouse effect (radiative forcing) in the CO_2 concentration and the concavity of the log-utility function (Traeger 2023).

3.2 Optimal amount of CDR

Next we study the optimal quantities of CDR. We obtain the following result:

Proposition 1. *The optimal level of carbon removed from reservoir j and stored in reservoir i is given by*

$$G^*_{i,j,t} = {f'_{i,j}}^{-1}\left(\frac{\overbrace{\beta\,\xi_0\left[(\mathbf{1}-\beta\,\mathbf{\Phi})^{-1}\right]_{1,j}}^{SCC_{M,j}} - \overbrace{\beta\,\xi_0\left[(\mathbf{1}-\beta\,\mathbf{\Phi})^{-1}\right]_{1,i}}^{SCC_{M,i}}}{\underbrace{\beta\,\xi_0\left[(\mathbf{1}-\beta\,\mathbf{\Phi})^{-1}\right]_{1,1}}_{SCC_{M,1}} + \underbrace{(1-\beta\,\kappa)\beta^{-t}\varphi_{R,0}}_{Hotelling\ rent} + \underbrace{\gamma_t}_{energy\ cost}}\right). \tag{13}$$

Proof. See Appendix B. □

As before, $[\cdot]_{1,i}$ ($[\cdot]_{1,j}$) denotes the i^{th} (j^{th}) element of the first row of the inverted matrix in square brackets and ${f'_{i,j}}^{-1}$ is the inverse of the marginal energy intensity of CDR from reservoir j with storage in reservoir i.

The optimal level of CDR with storage in any reservoir is a function of model parameters and the endogenously determined shadow value of the resource stock, which grows monotonically over time. As the marginal energy costs of CDR $f'_{i,j}(G_{i,j,t})$ are increasing, also its inverse ${f'_{i,j}}^{-1}$ is an increasing function. In particular, if the argument of ${f'_{i,j}}^{-1}$ is non-positive, the optimal amount of carbon removed from j and stored in i is zero. The

amount of CDR from j to i is positive only if

$$\left[(\mathbf{1} - \beta\,\mathbf{\Phi})^{-1}\right]_{1,j} > \left[(\mathbf{1} - \beta\,\mathbf{\Phi})^{-1}\right]_{1,i} \quad \text{for all} \quad i > 1 \quad \text{and} \quad j > 0.$$

This condition means that the social cost of carbon in the sink reservoir i is less than in the source reservoir i, i.e., that CDR measures are valuable by transferring carbon into a less damaging reservoir (less direct or indirect exchange with the atmosphere). The larger this value difference, the higher the optimal amount of CDR from j with storage in i.

The optimal amount of CDR decreases in the cost of energy production, reflected in the parameter γ_t and the Hotelling scarcity rent of fossil fuels. As γ_t falls over time, optimal CDR tends to increase over time. At the same time, the scarcity rent of fossil fuels grows over time, which counteracts the production cost effect.

In case of a quadratic energy cost function, ${f'_{i,j}}^{-1}$ is linear. As a result, the optimal level of CDR from reservoir j with storage in reservoir i is simply inversely proportional to its marginal costs. By contrast, in the case of a linear-quadratic cost function (as used in our numerical section), the optimal deployment can exhibit boundary solutions. CDR may be zero in early periods and only become positive at later points in time.

In summary, the core driver of CDR from reservoir j with storage in reservoir i is the relative difference in the SCC in these two reservoirs, which depends on transition rates, leakage, and discounting. As long as energy production depends on fossil fuels, Hotelling's rule predicts an increasing price of the fossil input suggesting that the optimal amount of CDR should fall over time. However, this increase is at least partially offset by energy production becoming more efficient and cheaper over time. Of course, if marginal costs of CDR from reservoir j with storage in reservoir i decrease over time as a result of (exogeneous) technological progress, optimal CDR would increase over time.

3.3 Implications of CDR for emissions and energy use

We next examine how CDR affects net emissions and gross energy use. As the purpose of CDR is to reduce the carbon stock in the atmosphere, we expect net emissions into the atmosphere to fall. At the same time, CDR uses energy and there is concern that, while reducing net emissions, CDR might lead to a substantial increase in overall gross energy use and gross emissions in the economy. Such an overall increase in energy use and gross emissions would crowd out some of the benefits of CDR, in particular, given that we are not fully eliminating carbon emissions but merely storing it away for some time with potential leakage. Given that we measure energy use in carbon equivalents, we find that optimal gross energy use and gross emissions are both given by E_t^*.

Proposition 2. *Optimal gross carbon emissions and gross energy use are*

$$E_t^* = \frac{v}{\underbrace{\beta\,\xi_0\,\left[(\mathbf{1}-\beta\,\mathbf{\Phi})^{-1}\right]_{1,1}}_{SCC} + \underbrace{(1-\beta\,\kappa)\beta^{-t}\varphi_{R,0}}_{Hotelling\ rent} + \underbrace{\gamma_t}_{energy\ cost}} + \sum_{i=2}^{r}\sum_{j=1}^{r} f_{i,j}\left(G_{i,j,t}^*\right), \quad (14)$$

where optimal CDR from reservoir j with storage in reservoir i, $G_{i,j,t}^*$, is given by equation (13)*. Moreover, optimal net emissions are* $E_t^{net*} = E_t^* - \sum_{i=2}^{r}\sum_{j=1}^{r} G_{i,j,t}^*$.

Proof. See Appendix C. □

The first term in equation (14) has some elements in common with the argument in equation (13), which describes the optimal amount of CDR. Whereas the optimal amount of CDR is crucially driven by the SCC difference between the reservoirs, here the core driver of emissions is the energy share of production v in the numerator. The influence of the energy share in production for gross energy use and emissions is adjusted by three terms in the denominator. The first expression in the denominator, the optimal emissions tax SCC_{M1}, lowers emissions. In the absence of the other terms in the denominator, a 1% increase in the carbon tax would lead to a 1% decrease of emissions. The second term in the denominator is the Hotelling rent, capturing how the intertemporal scarcity of fossil resources lowers optimal emissions. The third term in the denominator implies that the higher production costs of fossil-based energy reduce emissions and gross energy use. As in our discussion on optimal CDR, the Hotelling rent increases over time and reduces emissions, whereas the cost of energy production as a share of total output falls over time and increases emissions.

The second term in equation (14) captures the (direct) impact of CDR on gross emissions. It reflects the total energy use of CDR from all reservoirs with all storage reservoirs at the optimal levels given by equation (13) in Proposition 1. As we discussed there, also this second contribution to gross emissions and energy use falls with the Hotelling rent and the direct cost of energy.

However, this second term increases with a worsening of climate change as reflected in an increase in the damage parameter ξ_0. Thus, with CDR, the impact of higher climate change damages has an ambiguous effect on gross energy use. First, it reduces emissions by increasing the SCC, but second, it increases CDR and the energy use for CDR.

We obtain net emissions by subtracting the sum of optimal CDR across all storage options from gross emissions. Thus, the sum of carbon removed from the atmosphere net of the emission increase caused by the total energy used for CDR with its various storage

options is

$$\sum_{i=2}^{r}\sum_{j=1}^{r} G^*_{i,j,t} - f_{i,j}\left(G^*_{i,j,t}\right). \tag{15}$$

As optimality of CDR implies $f_{i,j}\left(G^*_{i,j,t}\right) < G^*_{i,j,t}$, i.e., it cannot be optimal to 'spend' more emissions on CDR than CDR extracts from the atmosphere, expression (15) will always be positive implying a net removal of atmospheric carbon.

Yet, equation (15) does not reflect the full net effect of CDR on emissions. Returning to equation (14) for gross energy use, CDR also has an indirect effect on the first term. By making energy use more valuable, CDR increases the value of fossil use, which increases the scarcity rent of fossil fuels.

Proposition 3. *Using CDR increases the shadow value of fossil fuels $\varphi_{R,0}$ and reduces net energy input into final good production, which is given by*

$$I^*_t = \frac{v}{\beta\,\xi_0\,\left[(\mathbf{1}-\beta\,\mathbf{\Phi})^{-1}\right]_{1,1} + (1-\beta\,\kappa)\beta^{1-t}\varphi_{R,0} + \gamma_t}. \tag{16}$$

Proof. See Appendix D. □

By increasing the Hotelling rent $\varphi_{R,0}$, CDR cuts net emissions further than equation (15) would suggest. This is a crucial difference between mitigation of emissions and CDR: Implementing a carbon carbon tax in order to mitigate emissions will reduce the scarcity of fossil fuels and, thereby, reduces the Hotelling rent. In our quantitative analysis, the optimal carbon tax will reduce the Hotelling rent by approximately 85%, compared to business as usual scenario. Such a reduction of the Hotelling rent implies an increase in fossil use or a partial crowd-out of the initial policy measure.

By contrast, the introduction of CDR increases the value of energy use and, thus, increases the Hotelling rent. In our quantitative analysis, we find that combined CDR deployment approximately doubles the Hotelling rent, thus additionally reducing emissions.

The direct costs of CDR reduce present (net) output. At the same time, CDR reduces the atmospheric carbon concentration, reducing future climate damages and increasing net output in the long run.

3.4 Including renewable energies

We now integrate our analysis of CDR with the green transition in the energy sector. Gross energy is composed of both fossil and renewable sources with endogeneous shares. We consider fossil and renewable energy as imperfect substitutes, such that gross energy is given by a constant-elasticity-of-substitution (CES) production function with fossil

inputs, $E_{f,t}$, and renewable, or 'green', inputs, $E_{g,t}$,

$$E_t = \left(aA_{f,t}^s E_{f,t}^s + (1-a)E_{g,t}^s\right)^{\frac{1}{s}}, \tag{17}$$

where the parameter $s < 1$ determines the elasticity of substitution, $\sigma = \frac{1}{1-s}$. A positive (negative) value for s corresponds to an elasticity of substitution larger (smaller) than one, reflecting substitutes (complements). The parameter $0 < a < 1$ measures the relative energy efficiency of the different energy sources.

With this generalized mode, we obtain the following formula for optimal CDR from reservoir j with storage in reservoir i (see Appendix F)

$$G_{i,j,t}^* = {f'_{i,j}}^{-1}\left(\frac{\overbrace{\beta\,\xi_0\left[(\mathbf{1}-\beta\,\mathbf{\Phi})^{-1}\right]_{1,j} - \beta\,\xi_0\left[(\mathbf{1}-\beta\,\mathbf{\Phi})^{-1}\right]_{1,i}}^{\text{savings in SCC by moving carbon from reservoir } j \text{ to reservoir } i}}{\left(\underbrace{\beta\,\xi_0\left[(\mathbf{1}-\beta\,\mathbf{\Phi})^{-1}\right]_{1,1}}_{\text{SCC}_{M,1}} + \underbrace{(1-\beta\,\kappa)\beta^{-t}\varphi_{R,0}}_{\text{Hotelling rent}}\right)\underbrace{\frac{1}{aA_{f,t}^s}\left(\frac{E_{f,t}}{E_t}\right)^{1-s}}_{\text{energy transition}} + \underbrace{\gamma_t}_{\text{energy cost}}}\right). \tag{18}$$

As compared to the result with only fossil energy in Proposition 1, equation (18) contains an 'energy transition' term in the denominator. The term inside brackets, $E_{f,t}^*/E_t^*$, characterizes the emission intensity of gross energy production. The higher the share of fossil fuels in the energy mix, the lower the optimal amount of CDR. The 'energy transition' term rescales only the social costs link to fossil use, i.e., $SCC_{M,1}$ and Hotelling rent. The mere production costs of energy, γ_t, are not affected. As a result, these direct energy production costs matter more for the optimal CDR deployment the cleaner the production mix (small $E_{f,t}$).

To understand the impact of the green transition on optimal CDR use in more detail, we use the expression (17) for gross energy use E_t in the 'energy transition' term, which becomes

$$aA_{f,t}^s\left(\frac{E_{f,t}}{E_t}\right)^{s-1} = aA_{f,t}\left(a + (1-a)\left(\frac{E_{g,t}}{A_{f,t}E_{f,t}}\right)^s\right)^{\frac{1-s}{s}}. \tag{19}$$

In this formulation, $E_{g,t}/\left(A_{f,t}E_{f,t}\right)$ is the efficiency-weighted ratio of green to dirty energy, which co-determines the optimal amount of CDR. The impact of this ratio is larger for more complementary energy inputs (larger $1-s$). In the limiting case of perfect substitutability ($s \to 1$), the input ratio no longer matters for the level of optimal CDR. This finding reflects how CDR's net effect on emission reductions relies not only on the effectiveness of sequestering carbon and its social value, but also on the implied increase in emissions through energy use.

The exogenous technological progress $aA^s_{f,t}$ governing fossil-based energy production has two impacts. First, more efficiently converting fossil fuels into usable energy cleans up energy production and increases optimal CDR (intensive margin). This effect is represented by the first appearance of $A_{f,t}$ on the right of equation (19). Second, as long as green and fossil energy are imperfect substitutes, technological progress in the fossil sector also increases the fossil share in the energy mix (extensive margin). This increase in fossil energy counteracts the efficiency increase and reduces the increase of CDR as a result of more efficient fossil technologies. If substitutability is sufficiently limited, the extensive margin effect can dominate the impact of the intensive margin and an efficiency increase in fossil energy can reduce the optimal level of CDR. Of course, during the green transition, we expect the technological progress in green energy ($E_{g,t}$) to dominate that of dirty energy. As a result, technological progress in fossil is not expected to increase the overall share of fossil energy, but merely to slow down the transition.

The following sections illustrate the previous theoretical findings. We first present the calibration and then the results. We focus on the climate-economy model including renewable energies as modeled in Section 3.4.

4 Model Calibration

We assume for all simulations to start in t = 2020 and end in t = 2400 with one period representing ten years, a standard assumption in the literature. However, given the distortions caused by the COVID-19 shock in 2020, we rely for the calibration on data obtained as the average from 2018 to 2022 rather than using 2020 data alone. We present first the calibration of the baseline-economy model without CDR and then present the inclusion of CDR.

4.1 Climate-Economy model without CDR (Baseline)

Initial output is set to 85.66 trillion (trn) USD/year (in 2015 prices), i.e., 856.64 trillion/decade. Economic growth is driven by increasing total factor productivity (TFP) A_t, which develops exogenously over time according to

$$A_{t+1} = A_t \left(1 + w_t\right)^{10}, \tag{20}$$

with

$$w_{t+1} = \frac{w_t}{\left(1 + d_w\right)^{10}}. \tag{21}$$

The initial growth rate of total factor productivity is assumed to be 1.5% per year, $w_{2020} = 0.015$, and the decline rate is $d_w = 0.0012$.

We use the same share of capital, $\kappa = 0.3$, as in Golosov et al. (2014) but select a higher

energy share, $v = 0.08$, based on Casey (2024). The utility discount rate is set to 1.4% per year (Traeger 2023). The given parameter set implies an optimal constant savings rate of $1 - x \approx 0.25$. The initial capital stock is set to 171.33 trn USD, approximately the output of two years, and fully depreciates over the course of a decade. The initial population is set to 7.73 billion and assumed to grow logistically over time to a maximum of 10.36 billion in 2200 as in Gerlagh and Liski (2018).

Energy production is described by the constant elasticity of substitution (CES) function specified in equation (17). In that equation, the parameter a measures the relative energy-efficiency of the different energy sources. We calculate the share parameter based on quantity and price data for fossil and renewable energies which leads to $a = 0.38$ and assume $s = 0.5$ based on Papageorgiou et al. (2017), Stöckl and Zerrahn (2023) and Golosov et al. (2014), leading to an elasticity of substitution of 2.0 between the clean and the dirty energy inputs. Using quantity and price data for fossil and renewable energies (see Appendix G.1) and data from the World Bank (2024) on resource rents for oil, coal and gas, we calibrate the energy cost coefficient γ from equation (9), $\gamma_{2020} = 0.011\%$ GDP/EJ. The energy cost parameter translates quantities into a fraction of GDP and, thus, falls over time along with TFP growth. The calibration of energy production and the corresponding share and cost parameters are detailed in Appendix G.1.

We measure energy in the same unit as emissions, gigatonnes of carbon (GtC). We use data on global energy supply from International Energy Agency (2024). The total global energy supply in 2020 is $I_{2020} = 602.85$ EJ, consisting of fossil energy in the amount of 489.65 EJ and renewable in the amount of 113.20 EJ. The carbon emissions from energy combustion and industrial processes in 2020 are 9.82 GtC (Global Carbon Project 2024). Based on fossil energy and carbon emissions we calculate the conversion factor $B = 49.85$ EJ/GtC.

The growth of renewable energy over time is characterized by

$$E_{g,t+1} = E_{g,t}\,(1 + w_{g,t})^{10}.$$

According to International Energy Agency (2024) data, renewable energy supply grew approximately 2% per year from 2010 to 2020. Thus, we set $w_{g,2020} = 0.02$. Similar to TFP growth, we let the growth rate of renewable energy decline over time according to

$$w_{g,t+1} = \frac{w_{g,t}}{(1 + d_g)^{10}}.$$

We choose the same decline rate for renewable energy growth as for TFP growth, $d_g = 0.0012$.

Plugging all values into equation (17) allows to calculate $A_I = 1.63$. We can now solve for the initial level of total factor productivity in equation (1), which delivers

$A_{2020} = 25.68$. We then use the model specification without climate damages to calibrate the initial resource stock of fossil fuels such that model emissions match the observed emissions of 2020, implying an initial fossil fuel stock of 1,110 GtC. Table 1 summarizes the model parameters and initial stock values.

A_{2020}	K_{2020}	N_{2020}	R_{2020}	κ	v	β	ξ_0
25.68	171.33 *trn USD*	7.73 *bn*	1,110 *GtC*	0.3	0.08	0.986 *1/year*	5.3×10^{-5} *1/GtC*
A_I	$w_{g,2020}$	d_g	w_{2020}	d_w	s	a	γ
1.63	0.02 *1/year*	0.0012 *1/year*	0.015 *1/year*	0.0012 *1/year*	0.5	0.38	0.011 *% GDP/EJ*

Table 1: Parameter values of the baseline climate-economy model

The increase in atmospheric carbon concentration due to emissions $E_{f,t}$ is determined by a linear three-box carbon cycle model. These "DICE-type" carbon cycle models have been criticized for omitting non-linear carbon cycle dynamics (Dietz et al. 2021), resulting for example in a decreasing ocean sink capacity in dependence of cumulative emissions (Sarmiento and Gruber 2006). However, Folini et al. (2025) show that this criticism is better explained by a lack of careful calibration than by the structure of these models and in turn provide a calibration that is in reasonable agreement with a multi earth system model ensemble (CMIP5). We rely on the main calibration of Folini et al. (2025) ("CDICE") and present additional results for their more extreme slow- and fast-sink calibrations ("LOVECLIM" and "MESMO", respectively) in Appendix H. These calibrations result in an equilibrium fraction of anthropogenic carbon ending up in the atmosphere of 26, 23, and 34 percent, for the average ("CDICE"), the fast ("LOVECLIM") and slow ("MESMO") sink calibration, respectively. Given our potential aggregated anthropogenic carbon perturbation of about 1,600 GtC we consider the average calibration ("CDICE") to be a reasonable fit, as Sarmiento and Gruber (2006) calculate a fraction of 21 percent for an anthropogenic perturbation of 1,800 GtC. We present the box model in more detail in the next section, where we explain the integration of CDR into the model.

Folini et al. (2025) provide initial carbon stocks for the year 2015. To obtain the initial states for 2020, we simulate the evolution of carbon stocks using historical emissions. Carbon flow parameters, adjusted from a 1 to a 10 year time step, and stock values in the year 2020 are summarized in Table 2.

We use a simple two-box energy balance model which translates radiative forcing into atmospheric and ocean temperature increase (T_t^{AT} and T_t^{OC}, respectively), using the multi-model mean calibration for CDICE from Folini et al. (2025). Radiative forcing results from increased atmospheric carbon concentration, $F_t^{CO_2}$, and exogenous forcing,

calibration	ϕ_{11}	ϕ_{12}	ϕ_{21}	ϕ_{22}	ϕ_{23}	ϕ_{32}	ϕ_{33}	M_1	M_2	M_3
CDICE	0.46	0.67	0.54	0.25	0.03	0.08	0.97	878	643	1,328
MESMO	0.41	1.17	0.59	-0.25	0.03	0.08	0.97	883	415	898
LOVECLIM	0.33	0.68	0.67	0.23	0.04	0.10	0.95	874	788	1,451

Table 2: Carbon cycle parameters for the three different calibrations (CDICE, LOVECLIM, and MESMO) obtained from Folini et al. (2025) (adjusted to a 10 year time step). Note that there is no direct transfer between M_1 and M_3, i.e. the atmosphere and the deep ocean, accordingly $\phi_{13} = \phi_{31} = 0$. The initial values for M_1, M_2, and M_3 in the year 2020 are obtained by adjusting the initial values in the year 2015 from Folini et al. (2025) using observed emissions since then.

F_t^{EX}. Following Folini et al. (2025) we assume the latter to be proportional to carbon radiative forcing (i.e., 0.3), such that total forcing is obtained as:

$$F_t = 1.3 \cdot F_{2\times CO_2} \frac{\ln(M_{1,t}/M_{1,pre})}{\ln 2} = 1.3 \cdot F_t^{CO_2}. \tag{22}$$

The corresponding increase in temperatures (above preindustrial levels) are determined by:

$$T_{t+1}^{AT} = T_t^{AT} + \Delta t\, c_1 \left(F_t - \lambda T_t^{AT} - c_3 \left(T_t^{AT} - T_t^{OC}\right)\right), \tag{23}$$

$$T_{t+1}^{OC} = T_t^{OC} + \Delta t\, c_4 \left(T_t^{AT} - T_t^{OC}\right) \tag{24}$$

with the parameters summarized in Table 3.

	c_1	c_3	c_4	λ	$F_{2\times CO_2}$	Δt	T_{2020}^{AT}	T_{2020}^{OC}
CDICE (MMM)	0.137	0.73	0.00689	1.06	3.45	1	1.32	0.30

Table 3: Temperature dynamics parameter values, obtained from the multi-model mean calibration (CDICE) from Folini et al. (2025).

Under these assumptions, business-as-usual output (i.e., in the absence of climate change damages) increases to 638.88 trn USD/yr by 2100 and annual gross energy provision to 1202.13 GJ/yr. This is in good agreement with the SSP2 scenario, as modelled by the MESSAGEix-GLOBIOM-1.2 model (Riahi et al. 2017; Byers et al. 2022). However, since our focus is on CDR deployment, our assumptions regarding renewable energy imply a more optimistic (exogenous) renewable growth path than in the SSP2 baseline scenario, with renewables reaching a share of 43 percent compared to about 20 percent in the baseline specification. Accordingly, atmospheric carbon concentration increases in our BAU scenario to 1,247 GtC (588 ppm), translating into a total forcing of 4.66 W/m^2, and a temperature increase of 3.03° by the year 2100.

Climate change damages are expressed as a share of global GDP and modeled as a function of atmospheric carbon concentration, as defined in equation (7). For the initial analysis, we choose the climate change damage parameter from Golosov et al. (2014), $\xi_0 = 5.3 \times 10^{-5}$. With this parameterization, our BAU atmospheric carbon concentration in the year 2100 implies a 3.33 percent loss in output. As alternative specification, we investigate in section 5.3 a higher climate damage parameter, $\xi_h = 10.8 \times 10^{-5}$, calibrated against the damage estimate from Howard and Sterner (2017), implying that damages increase to 6.68 percent of output for the BAU scenario in the year 2100. The calibration is detailed in Appendix G.2, which also describes an alternative damage function specification that is quadratic in temperature as an additional robustness check. Given our functional form for climate damages and to ensure a proper representation of high-damage outcomes, we impose the following constraint on atmospheric carbon concentration, $M_{1,t} >= M_{1,pre}$, which differs from the analytical model. We investigate in Section 5.2 how analytic and numeric results differ due to this assumption.

4.2 Climate-Economy model with CDR

4.2.1 CDR approaches

We distinguish between three different, rather generic CDR approaches. In the first approach, carbon is directly removed from the atmosphere and then geologically stored. We consider direct air carbon capture and storage (DACCS) as potential technology for the calibration of this approach.

In the second approach, the capacity of the ocean carbon sink is increased by chemically enhancing its buffer capacity. This could be achieved by applying interventions to shift the chemical distribution of carbon in the upper ocean (dissolved inorganic carbon, DIC) from CO_2 to other chemical forms (bicarbonate HCO_3^- and CO_3^{2-}bicarbonate). Linear carbon cycle box-models assume implicitly a constant distribution of carbon between the different chemical forms. Under this assumption, it is sufficient to use the carbon cycle stock variables to represent only the portion of carbon that is dissolved as CO_2 in the ocean. Hence, we assume that carbon present as dissolved CO_2 is removed from the box representing the upper ocean by this approach. In turn the uptake of atmospheric carbon increases. We refer to this approach as chemical-based ocean CDR and consider ocean alkalinity enhancement (OAE) technologies as the basis for the calibration.

In the third approach, the capacity of the ocean carbon sink is temporarily increased by accelerating the downward flux of biological fixed carbon into the deep ocean. We assume that carbon is transferred from the box representing the upper ocean to the box representing the deep ocean under this approach and that in turn the uptake of atmospheric carbon (from the upper box) increases. We refer to this approach as biological-

based ocean CDR and consider ocean iron fertilization (OIF) technologies as the basis for the calibration.

Note that under the two latter, ocean-based, approaches, also the concentration of dissolved CO_2 in the upper ocean decreases relative to the concentration in the deep ocean which would imply that not only carbon from the atmosphere enters the upper ocean but also from the deep ocean, if the CDR intervention would be carried out at a carbon cycle equilibrium. However, our initial conditions represent already a carbon cycle disequilibrium where the relative concentration of dissolved CO_2 in the upper ocean is larger than in the deep ocean (due to the slow mixing) and hence the net flux into the deep ocean increases since the exchange of CO_2 between the atmosphere and the upper ocean is much faster. Nevertheless, for the same amount of removal from the upper ocean, the increase in the net flux into the deep ocean is lower for the third approach (OIF) than for the second approach (OAE), since the third approach does not increase the total storing capacity of dissolved CO_2 (in equilibrium) whereas the second approach does.

The three-box carbon cycle (i.e., the carbon stocks in the atmosphere, M_1, the upper ocean M_2, and in the deep ocean, M_3) together with the carbon stock in geological storage reservoir, M_4, are displayed in equation (25), showing also how the three different CDR approaches intervene in such a carbon cycle. Whereas DACCS obviously "directly" removes carbon from the atmosphere, the removal of atmospheric carbon by ocean-based approaches acts via the carbon cycle transition matrix. Note that we have included the geological storage reservoir in the transition matrix to allow for the possibility of leakage.[4]

$$\begin{pmatrix} M_{1,t+1} \\ M_{2,t+1} \\ M_{3,t+1} \\ M_{4,t+1} \end{pmatrix} = \mathbf{\Phi} \begin{pmatrix} M_{1,t} \\ M_{2,t} \\ M_{3,t} \\ M_{4,t} \end{pmatrix} + \begin{pmatrix} E_{t,f} \\ 0 \\ 0 \\ 0 \end{pmatrix} + \begin{pmatrix} -\mathbf{DACCS}_t \\ 0 \\ 0 \\ +\mathbf{DACCS}_t \end{pmatrix} + \begin{pmatrix} 0 \\ -\mathbf{OAE}_t \\ 0 \\ 0 \end{pmatrix} + \begin{pmatrix} 0 \\ -\mathbf{OIF}_t \\ +\mathbf{OIF}_t \\ 0 \end{pmatrix} \tag{25}$$

4. We remind the reader that CDR is represented by the general control variable $G_{i,j,t}$, which denotes carbon transferred from reservoir j to reservoir i at time t. DACCS corresponds to removal from the atmosphere (box 1) and storage in the geological reservoir (box 4) and is therefore given by $G_{4,1,t}$. OAE removes carbon from the carbon cycle without transferring it to another active reservoir; for notational consistency, it can be represented as $G_{a,2,t}$, where a denotes an auxiliary sink not connected to the four-box carbon cycle. Finally, OIF transfers carbon from box 2 to box 3 and is represented by $G_{3,2,t}$. For notational convenience, we refer to DACCS, OAE, and OIF directly in the remainder of the paper, rather than to their corresponding control variables $G_{i,j,t}$.

with

$$\mathbf{\Phi} = \begin{pmatrix} \phi_{11} & \phi_{12} & 0 & \phi_{14} \\ \phi_{21} & \phi_{22} & \phi_{23} & \phi_{24} \\ 0 & \phi_{32} & \phi_{33} & \phi_{34} \\ 0 & 0 & 0 & \phi_{44} \end{pmatrix} \tag{26}$$

The level of CDR under the different approaches is independent of the level of emissions. This is different for carbon capture and storage (CCS) applied to point-source emissions, which is inherently constrained by the level of emissions. Apart from this constraint, the carbon removal pathway is equivalent to DACCS. We also include the possibility of point-source CCS subject to the constraint $CCS_t \leq \omega E_{t,f}$ into our model, where ω specifies the capture rate. Mitterrutzner et al. (2026) report capture rates between 90 and 99 percent for point sources. We set $\omega = 0.9$, which places our assessment on the optimistic side, since our emissions measure $E_{t,f}$ is not restricted to point-source emissions. This assumption nevertheless allows for a straightforward comparison of the distinct characteristics of CCS relative to CDR.

For those CDR methods which achieve atmospheric carbon removal via enhancing the carbon sink, i.e. OAE and OIF, the net emissions, E_t^{net}, are calculated by

$$E_t^{\text{net}} = M_{1,t+1}^{prescribed} - (\phi_{11} M_{1,t}^{prescribed} + \phi_{12} M_{2,t} + \phi_{13} M_{3,t}), \tag{27}$$

where $M_{1,t}^{prescribed}$ represents the atmospheric carbon concentration time series obtained from the simulation with CDR. For DACCS, net emissions can be obtained as displayed in the analytical section in equation (5).

4.2.2 CDR costs

Following Kalkuhl et al. (2022) and Hoel (2025) we assume that the cost of CDR are convex. The literature presents estimates of the (annual) potential of CDR as ranges, reflecting economic, biophysical, and geological limitations. Consider for example a CDR approach based on OAE. While the underlying chemical processes are well understood, removal efficiency critically depends on the duration of air–sea exchange of the enhanced-alkalinity water, that is, on the mixing of the ocean surface layer with deeper layers, with equilibration kinetics further influenced by factors such as temperature. These conditions vary across the ocean in dependence of latitude and the season of alkalinity release and in turn also the removal efficiency (e.g. Zhou et al. 2025). Obviously, our "uniform" upper ocean in the thee-box model does not represent this regional variation. While the operational cost for a given OAE deployment site might be linear, extending the annual OAE deployment requires moving to less favorable regions or extending the deployment period which means encountering less favorable weather conditions. Accordingly, extending

OAE deployment in our representation of the upper ocean implies increasing marginal costs. A similar reasoning applies to OIF deployment which acts as efficient CDR approach in certain regions in the Southern Ocean but outside that region the removal efficiency becomes very low (or even negative) (Oschlies et al. 2010). Also for DACCS, we argue that increasing the amount of CDR implies extending deployment to less favorable regions with for example less renewable energies available implying higher cost by higher electricity prices or lower net removal efficiency (if also fossil energy inputs are used), larger carbon transport cost to suitable storage sites, and higher storage cost due to price effects (Klepper and Rickels 2014; Golombek et al. 2023).

We calibrate the convex cost function using a linear–quadratic specification,

$$f_{i,j}(G_{i,j,t}) = g_{1,t}^{i,j} \cdot (G_{i,j,t}) + g_2^{i,j} \cdot (G_{i,j,t})^2, \tag{28}$$

whereby the linear parameter $g_{1,t}^{i,j}$ determines the start-up cost for deploying CDR and the parameter $g_2^{i,j}$ signifies the limitations in deployment for a given period of time.

The cost function reflects the cost of CDR by loosing output via the amount of energy required (in exajoules) to remove a given quantity of carbon from box j and its potential storage in box i. We assume that the start-up cost potentially decrease over time due to technological progress,

$$g_{1,t+1}^{i,j} = g_{1,t}^{i,j} \cdot (1 - \delta_t)^{10}. \tag{29}$$

Similar to TFP growth, we let the rate of technological progress decline over time according to

$$\delta_{t+1} = \frac{\delta_t}{(1 + d_\delta)^{10}}. \tag{30}$$

Since the cost estimates for CDR technologies in the literature are highly uncertain and vary substantially across studies (Babiker et al. 2022), we consider three different scenarios for the parameter signifying the quadratic term in the cost function, determining the limitations in scaling-up CDR. We present the values obtained from the literature for calibration in Table 9 in Appendix G.3 with values transformed from \$/tCO_2 into \$/tC and from GtCO_2/year into GtC/year.

Note that values in the literature are presented as cost per tons of carbon removed from the atmosphere, obtained from aggregating the estimates for the various cost components and relating them to the modeled net amount of atmospheric carbon removal. Using these estimates from the literature to calibrate our CDR cost function for the two ocean-based approaches would overestimate the costs since we instead directly model the removal or transfer of carbon from the upper ocean (resulting subsequently in atmospheric carbon removal by increased ocean carbon uptake). Accordingly, we derive a correction factor by an idealized experiment. We start the carbon cycle in equilibrium (i.e. no net fluxes between the carbon reservoirs) and track the distribution of carbon following an impulse

emission of 100 GtC to the atmosphere, offset at the same time by an impulse removal or transfer of 100 GtC from the upper ocean carbon box. From the experiments, we use the ratios for each measure after 100 years to adjust the cost estimates, since most cost estimates relate removal costs to atmospheric carbon removal over this time horizon. We consider all three carbon cycle calibrations provided by Folini et al. (2025) but the variation is rather low and we therefore use the average ratios for correction (see Table 10 in Appendix G.3).

Applying the correction factors to the CDR cost estimates from Table 9 in Appendix G.3, we calibrate equation (28) to the two data points, i.e. the low potential, low cost and the high potential, high cost data point. The cost parameters are chosen such that the resulting GDP loss for the initial period aligns with the two data points. GDP loss for 2020 is given by

$$\begin{aligned}\Delta_{G_{i,j,2020}} &= Y_{2020}(G_{i,j,t}=0) - Y_{2020}(G_{i,j,2020}>0) \\ &= Y_{2020}(G_{i,j,t}=0)\left[1-\left(\frac{E_{2020}-f_{i,j}(G_{i,j,t})}{E_{2020}}\right)^{v}\right] \\ \implies f_{i,j}(G_{i,j,2020}) &= E_{2020}\left[1-\left(1-\frac{\Delta_{G_{i,j,2020}}}{Y_{2020}}\right)^{\frac{1}{v}}\right].\end{aligned} \tag{31}$$

	Cost parameter values		
CDR	$g_{1,2020}$	potential	g_2
DACCS	30.11	high	0.17557
		mid	0.27085
		low	0.27330
OAE	21.96	high	0.09879
		mid	0.16742
		low	0.37255
OIF	0	high	2.8032
		mid	20.8217
		low	22.7243
CCS	10.46	high	0.1226
		mid	0.2009
		low	0.2180

Table 4: Overview of the calibrated cost parameter values for the different CDR approaches and CCS.

The resulting parameters in Table 4 represent well the different characteristics of the different CDR approaches. Both, DACCS and OAE are technically rather complex CDR methods, requiring a significant amount of energy, expressed by rather high values for $g_{1,2020}$ (30.11 EJ/GtC and 21.96 EJ/GtC for DACCS and OAE, respectively). In contrast,

OIF requires rather little material and energy input, and in turn the start-up cost are zero. However, the annual potential of OIF is rather limited, reflected in high values for g_2 which even in the high potential scenario exceeds the values for DACCS and OAE in their respective low potential scenarios. Even though the decision to apply CDR in our model structure goes beyond the pure energy input, it should be noted that the values in Table 4, measured in EJ/GtC, are still within the range of energy requirement estimates found in the literature. For DACCS, Hanna et al. (2021) report initial energy requirements in the range of 23.44 EJ/GtC to 72.51 EJ/GtC which pontentially drop to 16.23 EJ/GtC and 42.79 EJ/GtC for low- and high temperature-gas DACCS processes and high temperature-hydrogen DACCS processes, respectively; Realmonte et al. (2019) report a range from 18.32 EJ/GtC to 38.10 EJ/GtC for all possible DACCS processes; and Trompoukis et al. (2025) report a range of 13.15EJ/GtC to 66.20 EJ/GtC for solid sorbent-based DAC-processes and 22.34EJ/GtC to 45.80 EJ/GtC for liquid sorbent-based DAC processes. Renforth (2019) discuss different OAE methods, including 5 different ocean liming design options, and 3 different electrochemical weathering options, reporting a range for energy requirement of 3.664EJ/GtC to 66EJ/GtC.

The lower (and potential future) values in the reported ranges for the energy requirements for DACCS and OAE are covered by our scenarios regarding technological progress. We consider three scenarios regarding the annual reduction of the initial start-up cost parameter, $g^{i,j}_{1,2020}$:

"fast" : $\delta = 3.00\%$ and $d_\delta = 0.0012$,

"slow" : $\delta = 1.50\%$ and $d_\delta = 0.0012$, and

"no" : $\delta = 0\%$ and $d_\delta = 0$.

In those scenarios with technological progress, the rate declines over time by d_δ as explained above. Under these scenarios, the average energy requirement for removing 5 GtC by DACCS decreases from 31.31 (SD: 0.24) EJ/GtC in the year 2020 to 15.35 (SD: 12.28) EJ/GtC in the year 2100. The average energy requirement for removing 5 GtC by OAE processes decreases from 23.02 (SD: 0.62) EJ/GtC in 2020 to 11.39 (SD: 8.99) EJ/GtC in 2100. Since our calibration implies that the start-up cost for OIF are zero (i.e. the scaling up is mainly determined by biophysical limits), we assume that there is no technological progress for this CDR approach.

We follow the same strategy to calibrate the costs for CCS, assuming again a convex cost function (see e.g. Figure 3 in De Luna et al. 2023). We use recent cost estimates for CCS, summarized in Table 11 in Appendix G.4 to obtain the cost parameters as displayed in Table 4. The obtained cost parameters imply only in slightly increasing cost function. Note that in the case of CCS our presentation of the costs in terms of energy units is less consistent with bottom-up energy estimates, which would imply a range of 1.98 to 4.75

EJ/GtC (for $g^{CCS}_{1,2020}$). Hence, here the "additional" energy implicitly represents the capital cost and in turn the loss in output. However, note that with technological progress, the average energy requirement for capturing 5 GtC by CCS decreases from 11.36 (SD: 0.22) EJ/GtC in 2020 to 5.82 (SD: 4.27) EJ/GtC in 2100 and in the most optimistic scenario even to 1.62 EJ/GtC. Accordingly, the potential of CCS for climate change mitigation is well represented in our scenario space.

With these assumptions on CDR and CCS, i.e., three scenarios regarding the potential and three scenarios regarding cost development, we consider in total 9 cost scenarios. Reported standard deviations (SD) reflect the dispersion across these scenarios.

5 Quantitative Results

5.1 Different removal pathways and non-permanent carbon storage

Figure 1 shows the optimal deployment of the three different CDR approaches and CCS over time under the baseline climate damage function, assuming that each option is available only individually as part of climate policy. As expected, the low start-up cost of OIF (since $g^{OIF}_1 = 0$) imply that this CDR technology is utilized right from the beginning. However, its removal potential is limited, and annual average deployment reaches only 0.35 GtC by 2200 (see Table 12 in Appendix H).

This pattern differs for OAE and DACCS. Both CDR approaches begin to be deployed around 2050 and, driven by technological progress, average annual deployment reaches 2.88 GtC for OAE and 2.68 GtC for DACCS by 2100, increasing further to 8.42 GtC and 8.64 GtC by 2200, respectively. The figure also highlights the contrast between CCS and DACCS. While CCS exhibits higher deployment levels initially due to lower costs, its deployment declines after 2100 as emissions decrease, thereby limiting the scope for further application.

Note that the deployment profiles shown in Figure 1 are explained not only by differences in operational costs, but also by differences in the efficiency of carbon removal pathways. Figure 2 shows the individual, optimal deployment scenarios for the different CDR approaches, assuming however, that all approaches have the same cost (using the calibrated cost function for DACCS). Given the same cost, DACCS is most efficient since it removes carbon directly from the atmosphere, compared to the two ocean-based approaches which remove atmospheric carbon by increasing ocean carbon uptake. Among these two ocean-based approaches, OAE is more efficient than OIF since OAE increases the storage capacity of the ocean whereas OIF "only" accelerates the downward flux of carbon into the deep ocean.

Obviously, the result that DACCS is most efficient among the three CDR approaches

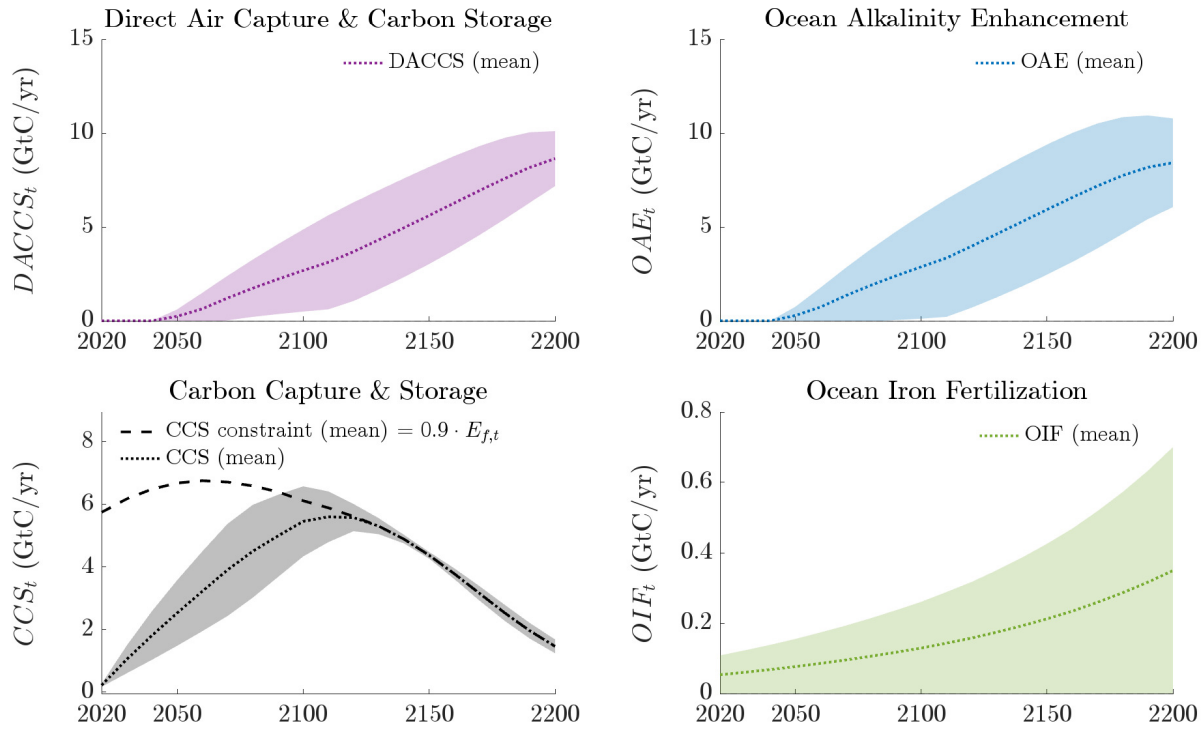

Figure 1: The use of various CDR methods and CCS when deployed individually as part of an optimal climate policy

in terms of the carbon removal pathway is based on the assumption of zero leakage from geological storage (i.e., $\phi_{14} = 0$), reflecting that storage sites are estimated to be relatively secure (Intergovernmental Panel on Climate Change 2005). Allowing for carbon leakage, i.e. assuming that DACCS provides only temporary instead of permanent removal, reduces its effectiveness. The upper panel in Figure 3 shows the mean, annual DACCS deployment in 2100 as a function of the leakage rate. While the optimal deployment reaches 2.68 GtC at a leakage rate of zero, it declines substantially to just 0.32 GtC if the leakage rate increases to 20%.

As shown in the theoretical analysis (Proposition 13), assuming a positive leakage rate (i.e., $\phi_{i4} > 0$) implies that the geological storage reservoir itself carries a shadow price, that is, a positive SCC. Accordingly, under leakage, geological storage does not differ from the other non-atmospheric carbon reservoirs in the carbon cycle. The lower panel of Figure 3 displays the carbon dynamics multipliers that govern differences in the SCC across reservoirs and illustrates how the multiplier for geological storage depends on the leakage rate ϕ_{14}. Since only the leakage rate of geological storage is varied, the carbon dynamics multipliers for the other reservoirs appear as straight lines and are determined by the parametrization of the three-box carbon cycle model following Folini et al. (2025).

The difference between the lines in Figure 3 indicate the benefits of CDR (see (13)

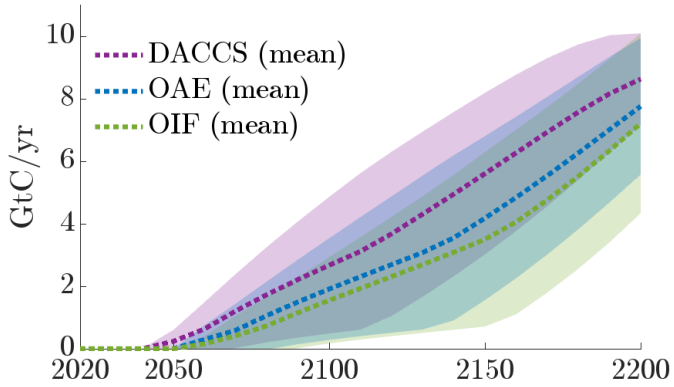

Figure 2: Optimal deployment of individual CDR approaches assuming identical costs, using the cost function derived for DACCS.

and (18)), i.e., in case of DACCS with geological storage, the difference between the atmospheric and the geological SCC. We see that this benefits falls quickly in the the leakage rate. Note that this applies also to CCS which differs from DACCS in its costs and is limited by the availability of emissions, but exhibits the same benefits from storage.

The benefit of OAE is given by the SCC of the upper ocean (which is "gained" by removing carbon from the upper ocean, but which is lower than the atmospheric SCC because of some inertia in the ocean carbon uptake). The benefit of OIF is given by the difference in the SCC of the upper and the deep ocean (i.e., the SCC of the upper ocean is "gained", however, incurring the SCC for the deep ocean).

Figure 3 shows that in the three box carbon cycle model with parametrization based on Folini et al. (2025), atmospheric carbon removal with deep ocean carbon injection and storage would be as effective as storage in a geological reservoir with a leakage rate of $\phi_{14} = 0.02$ in terms of climate change mitigation (ignoring any other possible impacts resulting from ocean carbon injection). Considering instead upper ocean carbon injection and storage would be approximately as effective as geological storage with a leakage rate of $\phi_{14} = 0.5$ in terms of climate change mitigation. For the all policy scenarios which include either CDR or CCS or both, the mean SCC are 44.14 (SD: 0.50) USD/tCO_2 in the year 2020. Hence, by removing a ton from the atmosphere and storing it geologically with a leakage rate of $\phi_{14} = 0.02$ (equivalent to deep ocean storage), the atmospheric SCC are "gained", but at the social cost of the storage reservoir, i.e. 5.96 (SD: 0.07) USD/tCO_2. Accordingly, the removal could be subsidizes by atmospheric SCC and the storage would be taxed by the storage SCC, or one would simply pay the net social benefit as subsidy, i.e., 39.18 (SD: 0.51) USD/tCO_2. Figure 8 in Appendix H shows the net carbon benefit for the different CDR methods.

Note that we have focused here on leakage directly to the atmosphere, however, various geological storage formation involve submarine storage, i.e., in the case of leakage, carbon would leak not to the atmosphere but to the deep ocean, $\phi_{34} > 0$, implying that the benefit

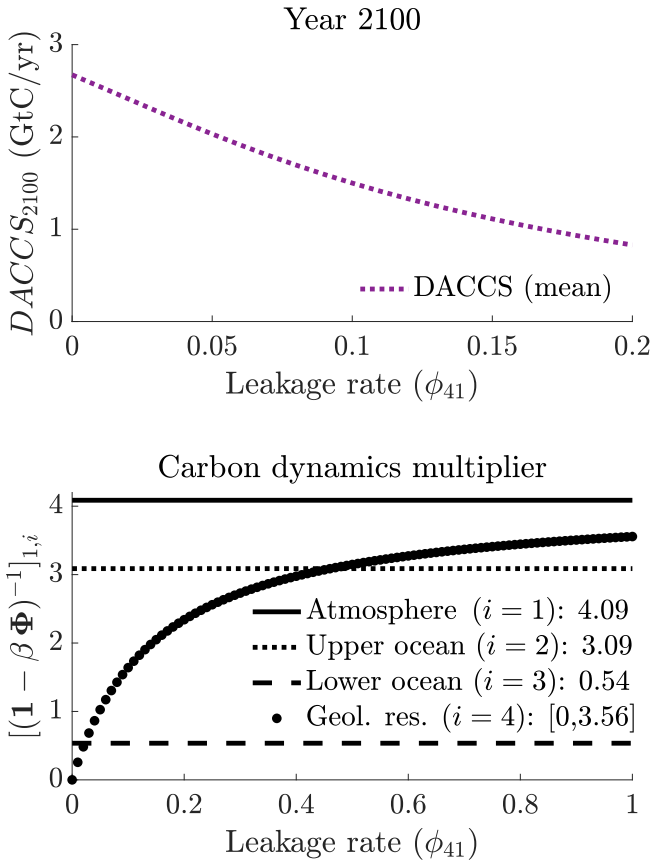

Figure 3: The benefits of temporary carbon storage. The upper panel shows optimal mean, annual DACCS deployment in the year 2100 as a function of the leakage rate of the geological reservoir. The lower panel shows the carbon dynamics multiplier as defined in equation (12) as a function of the leakage rate for the geological reservoir used for DACCS. Since variation in geological leakage does not affect rates of the carbon transfers between atmosphere, upper, and deep ocean, the carbon multipliers for these reservoirs are constant.

of such a leaky storage reservoir would increase significantly, since the already very low carbon multiplier of the deep ocean (see Figure 3) applies only to the small amount of leaked carbon. Considering the example from above, the social cost of leakage from a submarine geologic reservoir at a rate of $\phi_{34} = 0.02$ would be about 0.81 USD/tCO$_2$, implying that basically the full atmospheric SCC are gained as in the case of permanent storage.

However, this assessment of temporary storage (either resulting from a leaky reservoir or a reservoir in exchange with the atmosphere as it would be the case for ocean CDR or a combination, i.e., leaky submarine storage) is derived under a cost-benefit consideration allowing to postpone the impact on atmospheric carbon concentration but does not affect long-term carbon equilibria unless prevented by continuous CDR (Rickels and Lontzek 2012; Kalkuhl et al. 2022). Figure 9 in Appendix H shows the independence of long-run atmospheric carbon concentration in the case of temporary (ocean) carbon storage. The figure shows that full equilibration is achieved for the model calibration based on

Folini et al. (2025) for time horizon of 3000 years, irrespective if the carbon is released to the atmosphere or the deep ocean. This is because our simple three-box carbon cycle model ignores long-term carbon equilibration processes resulting from $CaCO_3$ and silicate weathering processes, which occur, for example, in response to interaction with marine sediments which restore the ocean's buffering capacity and its pH value on geological timescales (Broecker and Takahashi 1978; Ridgwell and Zeebe 2005).

The benefits of temporary carbon storage by postponing the impact on climate change becomes apparent by turning to the extreme case of full leakage. As a result of our 10 year time step, even full leakage still tucks carbon away for one decade, which explains why DACCS continues to have a small, but strictly positive value even at a leakage rate of 1 (see Groom and Venmans (2023) for a more comprehensive analysis of the time value of temporary carbon removal).

5.2 Interactions of CDR deployment with gross emissions and energy consumption

An optimal climate policy combines various CDR methods (Chiquier et al. 2025; Rodriguez Mendez et al. 2025). Therefore, it makes sense to examine the interactions for energy consumption and gross emissions in a combined scenario rather than for individual applications. Figure 4 shows optimal, combined deployment of DACCS, OAE, and OIF for the baseline climate damage function. The figure also shows the corresponding SCC, gross emissions, and net emissions. To put the change in net emissions into perspective, the figure displays the implications for atmospheric carbon concentration and temperature increase. These implications will be discuss in more detail in the next section where we include the alternative damage function and CCS.

In Appendix H we discuss the robustness of these results with respect to the damage function, showing results for a quadratic damage function, and with respect to the carbon cycle representation, showing the results for the different carbon cycle calibrations as detailed in Table 2.

Due to the convexity of the CDR cost, the deployment levels of each CDR methods decrease if all CDR methods are available compared to a situation where only the individual CDR method is available. Aggregated CDR deployment though is larger. However, this holds only true until the year 2200 from which onward the aggregated CDR deployment drops below the individual deployment level for both, DACCS and OAE (Table 12 in Appendix H) due to the feedback via energy consumption.

To detail the interactions and feedback at play in the deployment of CDR, Figure 5 shows how the different factors derived in (18) (Section 3.4) influence optimal deployment of DACCS. The corresponding information for the optimal deployment of OIF and OAE is shown in Figure 12 and 13 in Appendix H.

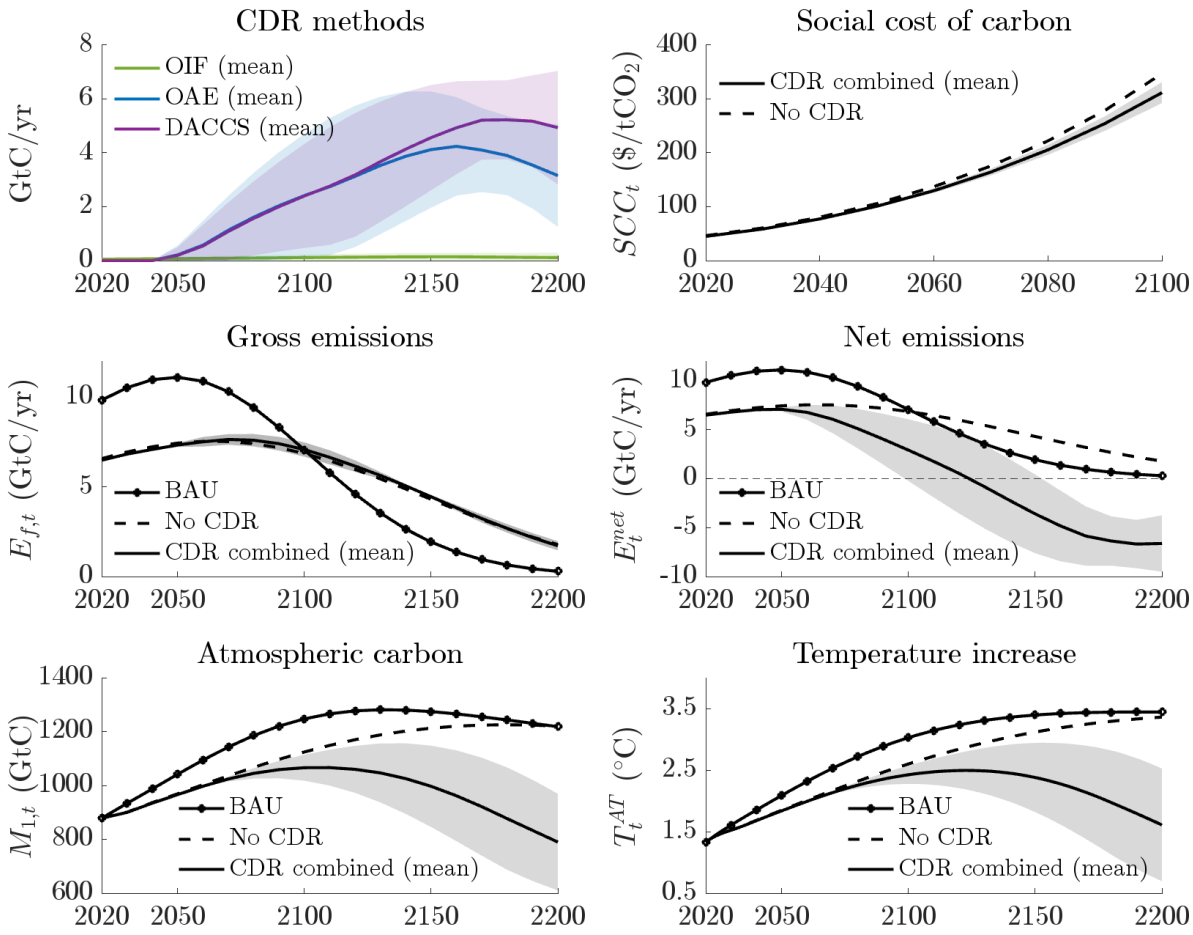

Figure 4: Optimal deployment of combined CDR for the baseline climate damage function

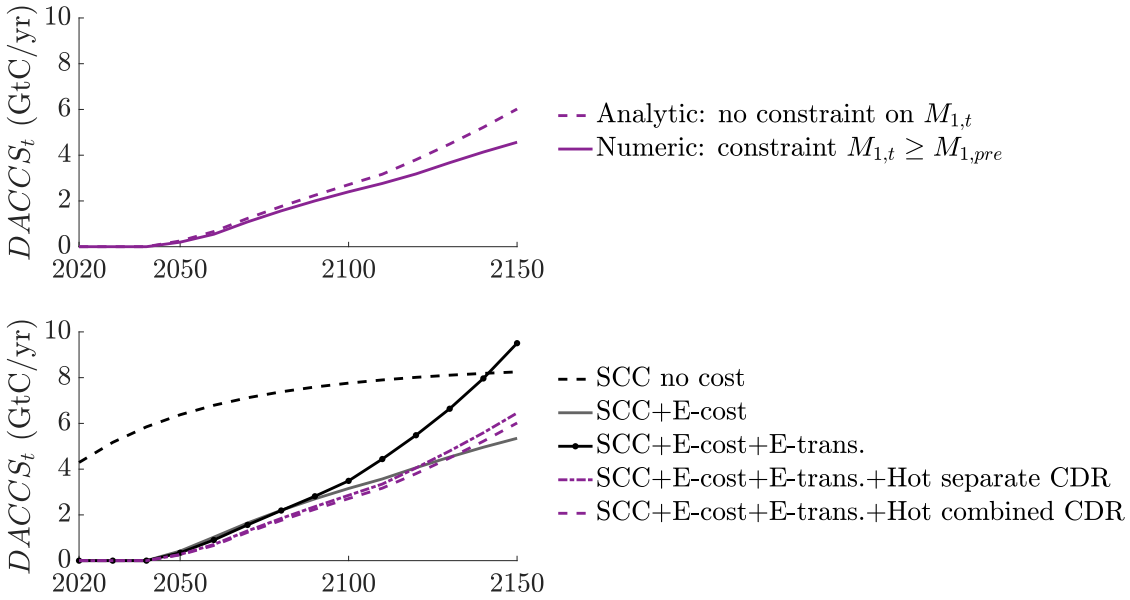

Figure 5: The upper graph show optimal DACCS deployment based on the analytical formula derived in equation (18) and the numerical outcome. The lower graph shows the different contributions to optimal DACCS deployment for the combined and individual case. The terms in the legend refer to the definitions in equation (18).

The upper panel in Figure 5 displays optimal DACCS deployment derived from the analytical expression in equation (18) and optimal DACCS deployment as part of the quantitative model solution. The observed difference arises from the constraint on atmospheric carbon concentration, $M_{1,t} >= M_{1,pre}$, which is introduced in the quantitative model. The results indicate that over the next 100 years, the analytical formula provides a close approximation to the constraint solution.

The lower panel of Figure 5 displays the contribution of the different factors determining CDR deployment, here focusing on DACCS, based on the theoretical decomposition in equation (18). When considering only the SCC components (i.e., abstracting from cost terms) in the numerator and denominator, the optimal deployment of DACCS with geological storage and no leakage increases moderately over time. This pattern reflects the rising SCC as well as declining deployment costs due to technological progress, while abstracting from direct energy production costs, fossil fuel scarcity, and the green energy transition.

Including additionally also direct energy cost ('SCC+E-cost'), DACCS deployment drops initially to zero, starting at low annual values around 2050. Subsequently, deployment increases as output grows and energy costs as a fraction of GDP decrease. Including also renewable energies ('SCC+E-cost+E-trans') raises optimal deployment considerably over time because with a decreasing share of fossil energy in the overall energy mix, the social cost impact of fossil use in CDR deployment measured by the SCC and the Hotelling rent decreases.

Still, even with increasing share of renewable energy provision, DACCS deployment also consumes fossil fuels, increasing therefore fossil fuel scarcity and the Hotelling rent compared to a climate policy without CDR (or CCS). This results in lower growth of DACCS and is even more pronounced in the combined CDR deployment case where also the other CDR methods contribute to fossil fuel scarcity (compare 'SCC+E-cost+E-trans+Hot separate CDR' and 'SCC+E-cost+E-trans+Hot combined CDR', respectively).

An increase in the Hotelling rent influences CDR deployment both directly and indirectly. The direct effect operates through the Hotelling term, which governs the deployment trajectory. Indirectly, a higher Hotelling rent alters the emissions profile of fossil fuels, thereby also affecting the energy transition component in equation (18).

While CDR methods are deployed only if they are net-negative, i.e., the amount of removal exceeds the emissions resulting from its deployment, the interaction with energy use is crucial for its impact on gross emissions. To demonstrate this effect, we vary the initial fossil resource stock: a higher initial stock implies a lower Hotelling rent, whereas a lower stock implies a higher rent. The left panel of Figure 6 shows the optimal carbon emissions in the year 2100 as a function of the initial fossil fuel resource stock. The right panel displays the difference in emissions between the no-CDR scenario and the CDR scenario, capturing the extent to which CDR increases gross emissions. At our benchmark fossil stock of 1,110 GtC, the emissions effect of CDR is minimal. However, as the initial stock increases, the effect becomes more pronounced. For instance, at an initial stock of 1,700 GtC, the introduction of CDR leads to an annual emissions increase of approximately 0.8 GtC in 2100.

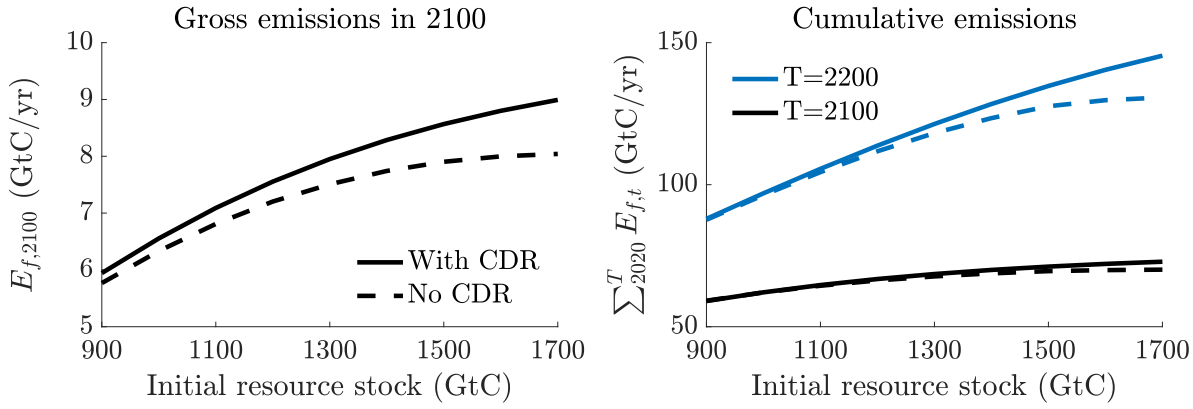

Figure 6: The graph shows carbon emissions (left) and the difference in emissions (right) in 2100 as a function of the initial resource stock for the model with combined CDR and without CDR.

However, the impact on gross emissions and the Hotelling rent is not only determined by the size of the fossil resource stock, but also by the climate policy in place. This can be seen by comparing the changes in gross emissions due to the inclusion of CDR and CCS in climate policy for the baseline and the high climate damage function as displayed

in Table 5. Note that in the table, the gross emissions for climate policies including CCS are shown 'before' capture, i.e., the impact of CCS on emissions is here treated like in the case for CDR to show the implications for (fossil) energy use. In terms of atmospheric carbon fluxes, CCS reduces gross and net emissions by the same amount.

Damages	Policy	2100		2200	
		Mean	pessimistic/ optimistic	Mean	pessimistic/ optimistic
Cumulative gross emissions by ... (in GtC)					
no	BAU	883		1105	
Baseline	woCDRwoCCS	646		1052	
	woCDRwCCS	640	636 / 661	1073	1027 / 1126
	wCDRwoCCS	649	631 / 678	1064	1029 / 1107
	wCDRwCCS	652	636 / 682	1057	958 / 1131
High	woCDRwoCCS	371		595	
	woCDRwCCS	521	466 / 601	1036	906 / 1168
	wCDRwoCCS	466	405 / 544	968	842 / 1066
	wCDRwCCS	561	479 / 608	1065	937 / 1171
Cumulative net emissions by ... (in GtC)					
no	BAU	883		1105	
Baseline	woCDRwoCCS	646		1052	
	woCDRwCCS	364	479 / 231	411	536 / 277
	wCDRwoCCS	522	630 / 339	174	768 / -447
	wCDRwCCS	318	491 / 126	-76	401 / -608
High	woCDRwoCCS	371		595	
	woCDRwCCS	95	125 / 74	147	169 / 130
	wCDRwoCCS	185	347 / -49	-233	287 / -856
	wCDRwCCS	-59	121 / -259	-322	33 / -777

Table 5: Cumulative gross and net emissions by the year 2100 and 2200 for the different policies. The policies differ whether they include (with, 'w') or exclude (without, 'wo') CDR and CCS. Only those climate policies with CDR and CCS include various scenarios, accordingly we display here also the results for the scenario with the most pessimistic and optimistic development of CDR and CCS costs. Note that for climate policies including CCS, the gross emissions are shown 'before' capture.

Under the baseline climate damage function, climate policy without CDR and without CCS primarily results in a smoothing of the emissions pathway. This is indicated by lower cumulative gross emissions by the year 2100 compared to BAU (237 GtC less). However, by 2200, the difference has shrunk to 55 GtC. And even though the Hotelling rents drops by about 70 percent in a climate policy without CDR and CCS compared to BAU, the fossil resource scarcity is somewhat limiting CDR and CCS and the implications on gross emissions is relative small. In a climate policy with CDR and with CDR and CCS, the

Hotelling rent drops by 66 and 55 percent, respectively. This is different for the high climate damage function where cumulative emissions drop considerably under climate policies without CDR and CCS, not only by 2100, but also by 2200 (dropping by 512 and 510 GtC, respectively). Now, the Hotelling rent drops to zero. In combination with an SCC that is approximately twice as high as under the baseline damage function, this leads to a significant use of CDR and CCS and a corresponding increase in gross emissions. The scarcity of fossil resources is now playing a role again (otherwise gross emissions would rise even stronger) and the Hotelling rent drops "only" by 83 percent and by 69 percent for climate policy with CDR and with CDR and CCS, respectively, compared to BAU.

Note that the increase in gross emissions is not equivalent to the share of energy used for CDR and CCS since the share of renewable energy provision is increasing over time. Table 13 in the Appendix shows the various climate policies, the cumulative amounts of CDR and CCS up to the years 2100 and 2200, and also the share in energy consumption in these two years. Under the high climate damage function, the share of energy consumption for CDR and CCS combined can increase to 19 percent (for the pessimistic scenario regarding the development of energy requirements for these technologies). Note that in the optimistic scenario, the share is 17 percent, while the mean share is 16 percent. Here, are two effects at play, in the pessimistic scenario, much less CDR and CCS is deployed (365 GtC by 2100), however, at a high energy burden. In the optimistic scenario, much more CDR and CCS is deployed (1100 GtC), at a low energy burden per ton, still translating into a higher share compared to the mean. Under the baseline climate damage function, the share is as expected lower (mean 8 percent, pessimistic scenario 5 percent, optimistic scenario 10 percent). However, this high share is not constant; by 2200, the average share drops significantly, especially for the high climate damage function (1 percent of energy consumption for CDR and CCS). The reason is that annual deployment levels by then have already considerably dropped (see also Table 12). This is because atmospheric carbon concentration has already considerably reduced, implying for our model specification that the constraint $M_1 \geq M_1^{pre}$ becomes binding or for a quadratic damage function that the climate change has essentially been resolved.

The impact on climate change is not determined by gross emissions, but by net emissions. The table shows the different impacts of various climate policies on net emissions. In climate policies without CDR and CCS, emissions are primarily shifted to the future for the baseline damage function, while they are significantly reduced for the high damage function. The addition of CCS can significantly reduce net emissions. The addition of CDR can even make it possible to achieve net-negative emissions. This is part of an optimal climate policy, especially for the high damage function, and the difference between a climate policy with CCS and without CDR is particularly clear when compared to a climate policy with CDR.

5.3 The effects of CDR for climate change mitigation

As already shown by Figure 4, the inclusion of CDR into climate policies result in temperature overshoot scenarios. Table 6 shows the implications for climate change mitigation of the different climate policies.

Damages	Policy	Net-zero year	Temperature increase in 2100	in 2200	Peak (Year)
no	BAU	–	3.03	3.44	3.44 (2192)
Baseline	woCDRwoCCS	–	2.60	3.36	3.36 (2200)
High	woCDRwoCCS	–	2.10	2.55	2.55 (2200)
Average development of CDR and CCS costs					
Baseline	woCDRwCCS	–	2.12	2.17	2.17 (2175)
	wCDRwoCCS	2124	2.42	1.61	2.49 (2122)
	wCDRwCCS	2093	2.06	0.96	2.07 (2093)
High	woCDRwCCS	–	1.52	1.60	1.60 (2200)
	wCDRwoCCS	2083	1.78	0.52	1.83 (2083)
	wCDRwCCS	2057	1.23	0.28	1.52 (2061)
Most optimistic development of CDR and CCS costs					
Baseline	woCDRwCCS	–	1.83	1.88	1.88 (2173)
	wCDRwoCCS	2087	2.13	0.46	2.16 (2090)
	wCDRwCCS	2075	1.68	0.38	1.84 (2072)
High	woCDRwCCS	–	1.46	1.54	1.54 (2191)
	wCDRwoCCS	2050	1.32	0.27	1.71 (2062)
	wCDRwCCS	2040	0.83	0.22	1.44 (2043)
Most pessimistic development of CDR and CCS costs					
Baseline	woCDRwCCS	–	2.34	2.43	2.44 (2172)
	wCDRwoCCS	2163	2.58	2.86	3.05 (2163)
	wCDRwCCS	2125	2.35	1.90	2.47 (2132)
High	woCDRwCCS	–	1.67	1.67	1.66 (2200)
	wCDRwoCCS	2125	2.08	1.16	2.12 (2121)
	wCDRwCCS	2085	1.62	0.37	1.64 (2084)

Table 6: Net-zero carbon emissions year and temperature increase above preindustrial for the different climate policies. The peak temperature is indicated for the time horizon up to the year 2200.

Without climate policy (BAU) our assumptions regarding the development of renewable energies and the size of the economically extractable fossil resource stock, temperature increase to 3.03°C and 3.44°C by the year 2100 and 2200, respectively. However, the majority of emissions will already have occurred by 2100 (see Table 5), and atmo-

spheric carbon concentrations will therefore already be declining before 2200, with peak temperature increases also slightly being reached before 2200, i.e., in the year 2192 (note the difference is not visible for two decimal places). For climate policies without CDR and CCS, temperature increase is reduced to 2.60°C and 2.10°C by the year 2100 for the baseline and high climate damage function, respectively. Including also CCS in climate policies, allows for further reducing the temperature increase by the year 2100, for average CCS cost development to 2.12°C and 1.52°C for baseline and high climate damages, respectively. However, in these scenarios temperature keeps increasing beyond the year 2100 and peak temperatures are approached at the end of the monitored period (i.e., the year 2200) and in the 2170s for climate policies without and with CCS, respectively.

Including also CDR into climate policies allows for achieving net-zero and net-negative carbon emissions. Table 6 shows that the possible net-zero years vary widely, depending on the assumption about climate damages, the assumptions about the cost development, and whether combined with CCS or not. For the most optimistic scenario regarding the cost development of CDR and CCS, net-zero emissions are achieved clearly before 2100, and for the high climate damages even before or at the year 2050. In these very ambitious climate policies under the assumption of optimistic cost development, peak increase in temperature is limited at 1.71°C and 1.44°C achieved in the year 2062 and 2043 for CDR climate policies with and without CCS, respectively. However, even under a pessimistic assumptions regarding the cost developments, combining CDR and CCS limits temperature increase to 1.64°C in the year 2084 under the assumption of high climate damages. Obviously, under baseline climate damages, deployment of CDR and CCS is less aggressive and the implemented climate policies lead to temperature increases of between 1.68°C and 2.35°C for optimistic and pessimistic cost developments, respectively.

6 Discussion and conclusion

Carbon dioxide removal (CDR) from the atmosphere, combined with storage in reservoirs outside the atmosphere, is required for ambitious climate policies in line with temperature targets of the Paris Agreement (Babiker et al. 2022). Whereas, without CDR, carbon dioxide emissions cause largely irreversible climate damage (Dietz and Venmans 2019), CDR opens up the possibility to 'clean up' past and on-going emissions of CO_2, and thus un-doing their climate damage. This distinguishes CDR from carbon capture and storage (CCS), an end-of-pipe technology that extracts the carbon dioxide from point source emissions and stores it in a reservoir outside the atmosphere. At the same time, the prospect of large-scale deployment of CDR has raised fundamental economic and policy concerns regarding its effectiveness and its role within an optimal climate policy portfolio.

Specifically, three concerns have featured prominently in the policy debate. First, the

availability of CDR may create a form of mitigation deterrence, if expectations of future removals weaken incentives to reduce emissions and slow the structural decarbonization of the economy. Second, most CDR technologies are energy intensive, raising concerns that removal could increase gross energy use and emissions, particularly when energy supply relies on fossil fuels. Third, carbon stored outside the atmosphere may not be permanently sequestered and could leak back over time, potentially creating a long-run obligation to repeatedly remove carbon and thereby reducing the net climate benefit of CDR.

This paper analyzes the key economic and carbon-cycle drivers that govern the role of carbon dioxide removal in optimal climate policy. We analyze CDR within an analytic climate-economy framework featuring energy use and an explicit multi-reservoir carbon cycle. This structure allows us to disentangle the general equilibrium and carbon-cycle feedbacks that underpin the main concerns surrounding CDR, while retaining sufficient transparency to derive closed-form analytical insights. We complement these analytical results with a calibrated quantitative analysis that illustrates the magnitude and timing of CDR deployment across alternative removal pathways and storage options.

Our analysis is conducted within a cost-benefit framework, with a particular emphasis on how different CDR pathways affect the SCC and optimal climate policy over time. We study both CDR and CCS, allowing us to compare atmospheric removal with point-source abatement within a unified framework. The calibrated quantitative analysis illustrates these mechanisms for three prominent CDR approaches, direct air capture, ocean alkalinity enhancement, and ocean iron fertilization, and contrasts them with CCS as a point-source abatement option. This combination of analytical and quantitative results provides a coherent basis for evaluating how CDR interacts with emissions pricing, energy use, and carbon storage over the transition to a low-carbon economy.

First, addressing concerns that the availability of CDR could weaken incentives for emissions reductions, we find that CDR does not materially change the optimal carbon price on emissions. Along the optimal path, the atmospheric social cost of carbon (SCC), and hence the optimal carbon tax, is nearly unaffected by the presence of CDR. This implies that the marginal incentives for emissions abatement remain largely intact even when CDR is available. In this sense, CDR differs fundamentally from geoengineering approaches such as solar radiation management, which can reduce the marginal damage from a unit of CO_2 emissions, thereby directly lowering abatement incentives. Our result does not imply that CDR is inexpensive or that it can substitute for decarbonization. Rather, it implies that efficient climate policy continues to require a high price on emissions, even in the presence of CDR. In the calibrated quantitative analysis, this translates into substantial emissions reductions alongside CDR deployment, with most CDR and CCS use occurring before and around the year 2100 under high climate damages, consistent with overshoot pathways in which atmospheric carbon concentrations are reduced

early.

Second, addressing concerns about energy use and rebound effects, we find that CDR can increase gross carbon dioxide emissions because removal itself requires energy. As long as energy supply relies partly on fossil inputs, this links CDR deployment to the intertemporal scarcity of fossil fuels. Higher energy demand associated with CDR raises the Hotelling scarcity rent, which by the Hotelling rule discourages current extraction and dampens the increase in gross emissions over time. Whether gross emissions rise or fall, therefore, depends on fossil fuel abundance and on the pace of the energy transition. When fossil resources are abundant and energy remains carbon intensive, the gross-emissions response to CDR is more pronounced, even though net emissions decline. As energy supply becomes cleaner and renewables increasingly substitute for fossil fuels, the emissions penalty of energy-intensive CDR falls and higher levels of CDR become optimal. In the calibrated model, these mechanisms translate into a substantial reduction in net emissions and peak temperatures when CDR and CCS are available. Under the baseline damage specification, temperature increases reach 3.36°C along the optimal path without CDR, whereas the integration of CDR and CCS limits average peak temperature increases to about 2.07°C, with peaks occurring earlier as part of an overshoot pathway rather than continuing to rise until the year 2200.

Third, differences in storage durability and leakage rates are a central determinant of the welfare value and optimal scale of CDR. In our framework, this role is captured by a shadow price wedge between the SCC in the atmosphere and the shadow value of carbon in the storage reservoir. With effectively permanent storage, the shadow value of stored carbon is close to zero, so removing one ton yields a benefit close to the atmospheric SCC. With non-permanent storage, or storage in reservoirs that exchange carbon with the atmosphere, this wedge narrows as leakage increases, reducing the net benefit of removal. This perspective clarifies why CDR options can differ markedly in their optimal deployment even when operational costs are similar: differences in storage pathways and carbon-cycle dynamics translate directly into differences in social value per ton removed. It also provides a transparent benchmark for policy design. Efficient implementation requires pricing emissions at the atmospheric SCC, while crediting verified removals by the atmospheric SCC net of the reservoir-specific shadow value, so that incentives explicitly reflect expected leakage and storage permanence.

In the calibrated model, these mechanisms imply meaningful differences across CDR technologies. Ocean alkalinity enhancement contributes at a scale comparable to direct air capture, reflecting its relatively durable storage pathway and moderate energy requirements. By contrast, the scope of ocean iron fertilization is too limited to materially alter the global path of net emissions under a coordinated, cost-benefit-optimal policy. CCS plays an important role in limiting the increase in atmospheric carbon concentrations by reducing gross emissions at point sources, but on its own it cannot generate cumulative

net-negative emissions and therefore primarily contributes to peak shaving rather than long-run carbon stock reduction. In scenarios with optimistic cost developments for CDR and CCS, net-zero emissions are achieved well before 2100, and under high climate damages, this occurs before or around mid-century. Direct air capture combined with deep ocean carbon injection is quantitatively comparable to geological storage with a leakage rate of about 0.02 per year in terms of climate mitigation effectiveness. Because many geological storage projects involve submarine reservoirs, such storage effectively retains most of the climate benefit of permanent removal even in the presence of small leakage rates.

Several caveats are important when interpreting these results. The model is intentionally stylized, both in its economic structure and in its representation of the climate system and the carbon cycle. CDR and CCS deployment costs are represented by reduced-form convex functions, and the energy transition is treated as exogenous. We abstract from co-benefits and side effects of CDR deployment, such as changes in ocean chemistry or CO_2 fertilization, as well as from distributional and political economy considerations and from uncertainty in climate damages, costs, and leakage rates.

A central modeling choice concerns the representation of the carbon cycle. The carbon cycle is modeled as linear and therefore does not capture non-linear sink saturation, explicit storage capacity constraints, or long-run geochemical feedbacks. As a consequence, the fraction (though not the absolute level) of steady-state atmospheric carbon concentration is independent of cumulative emissions. While this limits the model's ability to represent very large or very long-run perturbations of the carbon cycle, it allows us to isolate and compare the key economic mechanisms governing different CDR pathways within a transparent and analytically tractable framework. Extending the analysis to incorporate uncertainty, endogenous energy and technology transitions, explicit storage constraints, and additional climate interventions such as solar radiation management would be valuable directions for future research.

Overall, the paper provides a tractable approach to analyze how CDR moves climate policy from gross to net carbon accounting. CDR is a complement to emissions reductions, not a substitute: it can help lower atmospheric CO_2 concentrations and manage overshoot climate change, but it does not eliminate the need for strong emission reductions, and its social value depends critically on the durability of storage and the carbon intensity of the energy system.

References

Anderson, Kevin, Holly Jean Buck, Lili Fuhr, Oliver Geden, Glen P Peters, and Eve Tamme. 2023. "Controversies of carbon dioxide removal." *Nature Reviews Earth & Environment,* 1–7.

Anderson, Soren, and Richard Newell. 2004. "Prospects for carbon capture and storage technologies." *Annual Review of Environment and Resources* 29:109–142.

Babiker, M., G. Berndes, K. Blok, B. Cohen, A. Cowie, O. Geden, V. Ginzburg, A. Leip, P. Smith, M. Sugiyama, and F. Yamba. 2022. "Cross-sectoral perspectives." In *Climate Change 2022: Mitigation of Climate Change.* Contribution of Working Group III to the Sixth Assessment Report of the Intergovernmental Panel on Climate Change. Cambridge, UK and New York, NY, USA: Cambridge University Press.

Barrage, Lint, and William Nordhaus. 2023. *Policies, Projections, and the Social Cost of Carbon: Results from the DICE-2023 Model.* Working Paper 31112. National Bureau of Economic Research. https://www.nber.org/papers/w31112.

Bennæs, Anders, Martin Skogset, Tormod Svorkdal, Kjetil Fagerholt, Lisa Herlicka, Frank Meisel, and Wilfried Rickels. 2023. "Designing Pipeline Networks for Carbon Capture and Storage of CO-Sources in Germany: An Industry Perspective." In *Logistics Management Conference,* 82–98. Springer Nature Switzerland.

Brad, Alina, and Etienne Schneider. 2025. "Carbon removal, mitigation deterrence and the politics of target separation: Evidence from the EU 2040 climate target negotiation." *Environmental Research Letters* 20:054074. https://doi.org/10.1088/1748-9326/add0c9.

Brandão, Miguel, Miko UF Kirschbaum, Annette L Cowie, and Susanne Vedel Hjuler. 2019. "Quantifying the climate change effects of bioenergy systems: Comparison of 15 impact assessment methods." *GCB Bioenergy* 11 (5): 727–743.

Brander, Matthew, Francisco Ascui, Vivian Scott, and Simon Tett. 2021. "Carbon accounting for negative emissions technologies." *Climate Policy* 21 (5): 699–717.

Broecker, W.S., and T. Takahashi. 1978. "Neutralization of fossil fuel CO_2 by marine calcium carbonate." In *The Fate of Fossil Fuel CO_2 in the Oceans,* edited by N.R. Andersen and A. Malahoff, 213–248. New York: Plenum.

Byers, Edwards, Volker Krey, Elmar Kriegler, Keywan Riahi, Roberto Schaeffer, et al. 2022. *AR6 Scenarios Database.* International Institute for Applied Systems Analysis. https://doi.org/10.5281/zenodo.5886911.

Casey, Gregory. 2024. "Energy Efficiency and Directed Technical Change: Implications for Climate Change Mitigation." *The Review of Economic Studies* 91 (1): 192–228.

Chiquier, Solene, Angelo Gurgel, Jennifer Morris, Yen-Heng Henry Chen, and Sergey Paltsev. 2025. "Integrated assessment of carbon dioxide removal portfolios: land, energy, and economic trade-offs for climate policy." *Environmental Research Letters* 20:024002.

De Luna, Phil, Luciano Di Fiori, Yinsheng Li, Alastair Nojek, and Brandon Stackhouse. 2023. *The world needs to capture, use, and store gigatons of CO2: Where and how?* McKinsey & Company, Oil and Gas Practice. https://www.mckinsey.com/industries/oil-and-gas/our-insights/the-world-needs-to-capture-use-and-store-gigatons-of-co2-where-and-how#/.

Dietz, Simon, Frederick van der Ploeg, Armon Rezai, and Frank Venmans. 2021. "Are Economists Getting Climate Dynamics Right and Does It Matter?" *Journal of the Association of Environmental and Resource Economists* 8 (5): 895–921.

Dietz, Simon, and Frank Venmans. 2019. "Cumulative carbon emissions and economic policy: In search of general principles." *Journal of Environmental Economics and Management* 96:108–129. https://doi.org/10.1016/j.jeem.2019.04.003.

Edenhofer, Ottmar, Max Franks, Friedemann Gruner, Mathias Kalkuhl, and Kai Lessmann. 2025. "The Economics of Carbon Dioxide Removal." *Annual Review of Resource Economics* 17:301–321.

Edenhofer, Ottmar, Max Franks, Matthias Kalkuhl, and Artur Runge-Metzger. 2023. *On the Governance of Carbon Dioxide Removal – A Public Economics Perspective.* Working Paper 10370. CESifo. https://ssrn.com/abstract=4422845.

Emerson, David, Laura E. Sofen, Alexander B. Michaud, Stephen D. Archer, and Benjamin S. Twining. 2024. "A cost model for ocean iron fertilization as a means of carbon dioxide removal that compares ship- and aerial-based delivery, and estimates verification costs." *Earth's Future* 12 (4): e2023EF003732.

Folini, Doris, Aleksandra Friedl, Felix Kübler, and Simon Scheidegger. 2025. "The climate in climate economics." *Review of Economic Studies* 92 (1): 299–338.

Forster, P., T. Storelvmo, K. Armour, W. Collins, J.-L. Dufresne, et al. 2021. "The Earth's Energy Budget, Climate Feedbacks, and Climate Sensitivity." In *Climate Change 2021: The Physical Science Basis,* edited by V. Masson-Delmotte, P. Zhai, A. Pirani, S.L. Connors, C. Péan, et al., 923–1054. Cambridge, United Kingdom and New York, NY, USA: Cambridge University Press. https://doi.org/10.1017/9781009157896.009.

Fridahl, Mathias, Felix Schenuit, Liv Lundberg, Kenneth Möllersten, Miranda Böttcher, Wilfried Rickels, and Anders Hansson. 2023. "Novel carbon dioxide removals techniques must be integrated into the European Union's climate policies." *Communication Earth & Environment* 4:459.

Galán-Martín, Ángel, Daniel Vázquez, Selene Cobo, Niall Mac Dowell, José Antonio Caballero, and Gonzalo Guillén-Gosálbez. 2021. "Delaying carbon dioxide removal in the European Union puts climate targets at risk." *Nature Communications* 12 (1): 6490.

Galik, Christopher S, Justin S Baker, Adam Daigneault, and Gregory Latta. 2022. "Crediting temporary forest carbon: Retrospective and empirical perspectives on accounting options." *Frontiers in Forests and Global Change* 5:933020.

Geden, Oliver, Glen P. Peters, and Vivian Scott. 2019. "Targeting carbon dioxide removal in the European Union." *Climate Policy* 19 (4): 487–494.

Gerlagh, Reyer, and Matti Liski. 2018. "Consistent climate policies." *Journal of the European Economic Association* 16 (1): 1–44.

Global Carbon Project. 2024. *Global Carbon Atlas.* http://www.globalcarbonatlas.org/en/CO2-emissions.

Golombek, Rolf, Mads Greaker, Snorre Kverndokk, and Lin Ma. 2023. "Policies to Promote Carbon Capture and Storage Technologies." *Environmental and Resource Economics* 85:267–302.

Golosov, Mikhail, John Hassler, Per Krusell, and Aleh Tsyvinski. 2014. "Optimal Taxes on Fossil Fuel in General Equilibrium." *Econometrica* 82 (1): 41–88.

Groom, Ben, and Frank Venmans. 2023. "The social value of offsets." *Nature* 619 (7971): 768–773.

Hanna, Ryan, Ahmed Abdulla, Yangyang Xu, and David G. Victor. 2021. "Emergency deployment of direct air capture as a response to the climate crisis." *Nature Communications* 12:368. https://doi.org/10.1038/s41467-020-20437-0.

Herzog, Howard, Ken Caldeira, and John Reilly. 2003. "An issue of permanence: Assessing the effectiveness of temporary carbon storage." *Climatic Change* 59 (3): 293–310.

Hoel, Michael. 2025. "The path to net zero emissions." *Journal of Environmental Economics and Management* 132:103177.

Howard, Peter H., and Thomas Sterner. 2017. "Few and Not So Far Between: A Meta-analysis of Climate Damage Estimates." *Environmental and Resource Economics* 68:197–225.

Intergovernmental Panel on Climate Change. 2005. *Special Report on Carbon Dioxide Capture and Storage.* Cambridge, United Kingdom and New York, NY, USA: Cambridge University Press.

International Energy Agency. 2024. *Energy Statistics Data Browser.* Paris. https://www.iea.org/data-and-statistics.

———. 2025. *Share of renewables in energy consumption, 2022.* https://www.iea.org/world/renewables.

International Renewable Energy Agency. 2024. *Global Trends.* https://www.irena.org/Data/View-data-by-topic/Costs/Global-Trends.

Kalkuhl, Matthias, Max Franks, Friedemann Gruner, Kai Lessmann, and Ottmar Edenhofer. 2022. *Pigou's Advice and Sisyphus' Warning: Carbon Pricing with Non-Permanent Carbon-Dioxide Removal.* Working Paper 10169. CESifo.

Karp, Larry. 2017. "Provision of a public good with multiple dynasties." *The Economic Journal* 127 (607): 2641–2664.

Kheshgi, Haroon S., and David E. Archer. 2004. "A nonlinear convolution model for the evasion of CO_2 injected into the deep ocean." *Journal of Geophysical Research: Oceans* 109 (C2).

Klepper, Gernot, and Wilfried Rickels. 2014. "Climate Engineering: Economic Considerations and Research Challenges." *Review of Environmental Economics and Policy* 8 (2): 270–289.

Kowalczyk, Katarzyna A., Thorben Amann, Jessica Strefler, Maria-Elena Vorrath, Jens Hartmann, Serena De Marco, Phil Renforth, Spyros Foteinis, and Elmar Kriegler. 2024. "Marine carbon dioxide removal by alkalinization should no longer be overlooked." *Environmental Research Letters* 19 (7): 074033.

Lafforgue, Gilles, Bertrand Magné, and Michel Moreaux. 2008. "Energy substitutions, climate change and carbon sinks." *Ecological Economics* 67 (4): 589–597.

Liu, Yi, JK Moore, F Primeau, and WL Wang. 2023. "Reduced CO2 uptake and growing nutrient sequestration from slowing overturning circulation." *Nature Climate Change* 13 (1): 83–90.

Meier, Felix D., and Christian P. Traeger. 2022. *SolACE – Solar Geoengineering in an Analytic Climate Economy.* https://papers.ssrn.com/sol3/papers.cfm?abstract_id=3958821.

Mitterrutzner, Benjamin, Benjamin K. Sovacool, Brage Rugstad Knudsen, Morgan D. Bazilian, Jinsoo Kim, Simon Roussanaly, Asgeir Tomasgard, and Steven Griffiths. 2026. "Scaling carbon capture and storage (CCS) to gigaton capacity: A multi-dimensional and critical review." *International Journal of Greenhouse Gas Control* 149:104531.

National Academies of Sciences, Engineering, and Medicine. 2021. *A research strategy for ocean-based carbon dioxide removal and sequestration.* https://nap.nationalacademies.org/catalog/26278/a-research-strategy-for-ocean-based-carbon-dioxide-removal-and-sequestration?utm_source=nationaltribune&utm_medium=nationaltribune&utm_campaign=news.

Nordhaus, William. 2007. "To Tax or Not to Tax: The Case for a Carbon Tax." *Review of Environmental Economics and Policy* 1 (1): 26–44.

Oschlies, Andreas, Wolfgang Koeve, Wilfried Rickels, and Katrin Rehdanz. 2010. "Side effects and accounting aspects of hypothetical large-scale Southern Ocean iron fertilization." *Biogeosciences* 7 (12): 4017–4035.

Papageorgiou, Chris, Marianne Saam, and Patrick Schulte. 2017. "Substitution between clean and dirty energy inputs: A macroeconomic perspective." *Review of Economics and Statistics* 99 (2): 281–290.

Parisa, Zack, Eric Marland, Brent Sohngen, Gregg Marland, and Jennifer Jenkins. 2022. "The time value of carbon storage." *Forest Policy and Economics* 144:102840.

Realmonte, Giulia, Laurent Drouet, Ajay Gambhir, James Glynn, Adam Hawkes, Alexandre C. Köberle, and Massimo Tavoni. 2019. "An inter-model assessment of the role of direct air capture in deep mitigation pathways." *Nature Communications* 10:3277.

Renforth, P. 2019. "The negative emission potential of alkaline materials." *Nature Communications* 10:1401. https://doi.org/10.1038/s41467-019-09475-5.

Renforth, Phil, Barrie G. Jenkins, and Tim Kruger. 2013. "Engineering challenges of ocean liming." *Energy* 60 (1): 442–452.

Riahi, Keywan, Detlef P. van Vuuren, Elmar Kriegler, Jae Edmonds, Brian C. O'Neill, et al. 2017. "The Shared Socioeconomic Pathways and their energy, land use, and greenhouse gas emissions implications: An overview." *Global Environmental Change* 42:153–168.

Rickels, Wilfried, and Thomas S. Lontzek. 2012. "Optimal global carbon management with ocean sequestration." *Oxford Economic Papers* 64 (2): 323–349.

Rickels, Wilfried, Roland Rothenstein, Felix Schenuit, and Mathias Fridahl. 2022. "Procure, bank, release: Carbon removal certificate reserves to manage carbon prices on the path net-zero." *Energy Research & Social Science* 94:102858.

Ridgwell, A., and R. E. Zeebe. 2005. "The role of the global carbonate cycle in the regulation and evolution of the Earth system." *Earth and Planetary Science Letters* 234 (3–4): 299–315.

Rodriguez Mendez, Quirina, Felix Creutzig, and Sabine Fuss. 2025. "Deep uncertainty in carbon dioxide removal portfolios." *Environmental Research Letters* 20 (5): 054013.

Rubin, Edward S., John E. Davison, and Howard J. Herzog. 2015. "The cost of CO_2 capture and storage." *International Journal of Greenhouse Gas Control* 40:378–400.

Sarmiento, Jorge L., and Nicolas Gruber. 2006. *Ocean Biogeochemical Dynamics.* Princeton and Oxford: Princeton University Press.

Sierra, Carlos A, Susan E Crow, Martin Heimann, Holger Metzler, and Ernst-Detlef Schulze. 2021. "The climate benefit of carbon sequestration." *Biogeosciences* 18 (3): 1029–1048.

Stöckl, Fabian, and Alexander Zerrahn. 2023. "Substituting clean for dirty energy: A bottom-up analysis." *Journal of the Association of Environmental and Resource Economists* 10 (3): 819–863.

Traeger, Christian P. 2021. *IAMs and CO_2 emissions – an analytic discussion.* Technical report. Mimeo.

———. 2023. "ACE – Analytic Climate Economy." *American Economic Journal: Economic Policy* 15 (3): 372–406.

Trompoukis, Christos, Kati Koponen, Jere Elfving, Alexander Deliukov, Andromachi Kila, Cyril Bajamundi, and Jan Bormans. 2025. *The role of Direct Air Capture technologies in the EU's decarbonisation effort.* Technical report PE 772.474. Policy Department for Transformation, Innovation, Health, Directorate-General for Economy, Transformation, and Industry.

World Bank. 2023. *Commodity Price Data.* https://thedocs.worldbank.org/en/doc/5d903e848db1d1b83e0ec8f744e55570-0350012021/related/CMO-Historical-Data-Annual.xlsx.

World Bank. 2024. *Natural Resource Rents.* https://databank.worldbank.org/source/adjusted-net-savings/Series/NY.GDP.TOTL.RT.ZS.

Young, John, Noah McQueen, Charithea Charalambous, Spyros Foteinis, Olivia Hawrot, Manuel Ojeda, Helene Pilorgé, John Andresen, Peter Psarras, Phil Renforth, Susana Garcia, and Mijndert van der Spek. 2023. "The cost of direct air capture and storage can be reduced via strategic deployment but is unlikely to fall below stated cost targets." *One Earth* 6, no. 7 (July): 899–917. https://doi.org/10.1016/j.oneear.2023.06.004.

Zhou, Mengyang, Michael D. Tyka, David T. Ho, Elizabeth Yankovsky, Scott Bachman, Thomas Nicholas, Alicia R. Karspeck, and Matthew C. Long. 2025. "Mapping the global variation in the efficiency of ocean alkalinity enhancement for carbon dioxide removal." *Nature Climate Change* 15 (1): 59–65.

Zwaan, Bob van der, and Reyer Gerlagh. 2009. "Economics of geological CO_2 storage and leakage." *Climatic Change* 93:285–309.

Appendices

A Solving the linear-in-states model

As the model developed here shares many features with Traeger (2023), especially the 'linear-in-states property' due to logarithmic utility, the Cobb-Douglas production function, full capital depreciation, and the linear carbon cycle, the derivation of results also has much in common with Traeger (2023). The consumption rate x_t is defined as consumption C_t over net production, given by equation (8):

$$x_t = \frac{C_t}{Y_t \left[1 - D_t\left(M_{1,t}\right)\right] \exp(-\gamma_t E_t)}.$$

Using $c_t = C_t/N_t$ to denote per-capita consumption, taking logs, and rearranging, we obtain

$$\log c_t = \log x_t + \log A_t + \kappa \log K_t - (\kappa + v) \log N_t + v \log I_t - \xi_0 \left(M_{1,t} - M_1^{pre}\right) - \gamma_t E_t.$$

We transform the optimization problem (10) into its dynamic programming form, with the Bellman equation given as

$$V(k_t, \boldsymbol{M}_t, R_t, t) = \max_{x_t, E_t, G_t} \Bigg\{ \log x_t + \log A_t + \kappa \log K_t - (\kappa + v) \log N_t \\ + v \log I_t(E_t, G_{i,j,t}) - \xi_0 \left(M_{1,t} - M_1^{pre}\right) - \gamma_t E_t + \beta\, V(k_{t+1}, \boldsymbol{M}_{t+1}, R_{t+1}, t+1) \Bigg\},$$

where $k_t = \log K_t$. The dynamics of log capital k_t are described by the equation of motion

$$\begin{aligned} k_{t+1} = &\log A_t + \kappa\, k_t + (-\kappa - v) \log N_t + v \log I_t \\ &- \xi_0 \left(M_{1,t} - M_1^{pre}\right) - \gamma_t E_t + \log(1 - x_t). \end{aligned} \tag{32}$$

To solve the Bellman equation, we guess that the value function can be written as

$$V(k_t, \boldsymbol{M}_t, R_t, t) = \varphi_k\, k_t + \boldsymbol{\varphi}_M^T\, \boldsymbol{M}_t + \varphi_{R,t}\, R_t + \varphi_t, \tag{33}$$

where the parameters φ_m, which are yet to be determined, denote the shadow values for the different states m, and a superscript ^{T} denotes the transpose of a vector of shadow values.

Inserting the guess and the next periods states (equations 2, 3, and 32) into the

Bellman equation delivers

$$
\begin{aligned}
&\varphi_k\, k_t + \boldsymbol{\varphi}_M^T\, \boldsymbol{M}_t + \varphi_{R,t}\, R_t + \varphi_t \\
&\quad = \max_{x_t, E_t, G_{i,j,t}} \Bigg\{ \log x_t + \log A_t + \kappa\, k_t - (\kappa + v) \log N_t + v \log I_t(E_t, G_{i,j,t}) \\
&\qquad - \xi_0\, (M_{1,t} - M_1^{pre}) - \gamma_t E_t + \beta\, \varphi_k \Big(\log A_t + \kappa\, k_t - (\kappa + v) \log N_t \\
&\qquad + v \log I_t(E_t, G_{i,j,t}) - \xi_0\, (M_{1,t} - M_1^{pre}) - \gamma_t E_t + \log(1 - x_t) \Big) \\
&\qquad\qquad + \beta\, \boldsymbol{\varphi}_M^T\, (\boldsymbol{\Phi} \boldsymbol{M}_t + \boldsymbol{E}_t) + \beta\, \varphi_{R,t+1}\, (R_t - E_t) + \beta\, \varphi_{t+1} \Bigg\}. \quad (34)
\end{aligned}
$$

As in equation (4), $\boldsymbol{E}_t$ is a vector that contains net emissions, and the net amounts of carbon transfers $G_{i,j,t}$.

First order conditions. Maximizing the right hand side of (34) over x_t yields

$$
\frac{1}{x_t} - \beta\, \varphi_k \frac{1}{1 - x_t} = 0 \quad \Longrightarrow \quad x_t^* = \frac{1}{1 + \beta\, \varphi_k}. \quad (35)
$$

The first order condition for CDR from reservoir j with storage in reservoir i can be written as

$$
-v(1 + \beta\, \varphi_k)\, \frac{f'_{i,t}(G_{i,j,t})}{I_t} = \beta(\varphi_{Mj} - \varphi_{Mi}), \quad (36)
$$

and the first order condition for gross emissions as

$$
v(1 + \beta\, \varphi_k)\, \frac{1}{I_t} = \beta(\varphi_{R,t+1} - \varphi_{M1}) + (1 + \beta\, \varphi_k)\gamma_t. \quad (37)
$$

Inserting (37) into (36) yields

$$
\begin{aligned}
& f'_{i,j}(G_{i,j,t})\, [\beta(\varphi_{R,t+1} - \varphi_{M1}) + (1 + \beta\, \varphi_k)\gamma_t] = -\beta(\varphi_{Mj} - \varphi_{Mi}) \\
\Leftrightarrow\ & f'_{i,j}(G_{i,j,t}) = -\frac{\beta(\varphi_{Mj} - \varphi_{Mi})}{\beta(\varphi_{R,t+1} - \varphi_{M1}) + (1 + \beta\, \varphi_k)\gamma_t} \\
\Leftrightarrow\ & G^*_{i,j,t} = {f'_{i,j}}^{-1} \left(\frac{\beta(-\varphi_{Mj} + \varphi_{Mi})}{\beta(\varphi_{R,t+1} - \varphi_{M1}) + (1 + \beta\, \varphi_k)\gamma_t} \right) \\
\Leftrightarrow\ & G^*_{i,j,t} = {f'_{i,j}}^{-1} \left(\frac{-\varphi_{Mj} + \varphi_{Mi}}{\varphi_{R,t+1} - \varphi_{M1} + \frac{(1+\beta\, \varphi_k)}{\beta}\gamma_t} \right) \\
\Leftrightarrow\ & G^*_{i,j,t} = {f'_{i,j}}^{-1} \left(\frac{-\varphi_{Mj} + \varphi_{Mi}}{\varphi_{R,t+1} - \varphi_{M1} + \Gamma_t} \right), \quad (38)
\end{aligned}
$$

where $\Gamma_t = \frac{(1+\beta\,\varphi_k)}{\beta}\gamma_t$ and the inverse of the marginal cost function is denoted by ${f'_{i,j}}^{-1}$. Summing up CDR deployment over all reservoir types yields

$$G_t^* = \sum_{i=2}^{r}\sum_{j=1}^{r} {f'_{i,j}}^{-1}\left(\frac{-\varphi_{Mj}+\varphi_{Mi}}{\varphi_{R,t+1}-\varphi_{M1}+\Gamma_t}\right).$$

We obtain optimal emissions solving equation (37)

$$\begin{aligned}
&v(1+\beta\,\varphi_k) = \left(E_t - \sum_{i=2}^{r}\sum_{j=1}^{r} f_{i,j}(G^*_{i,j,t})\right)\beta(\varphi_{R,t+1}-\varphi_{M1}) + (1+\beta\,\varphi_k)\gamma_t \\
\Leftrightarrow\; & E_t - \sum_{i=2}^{r}\sum_{j=1}^{r} f_{i,j}(G^*_{i,j,t}) = \frac{v(1+\beta\,\varphi_k)}{\beta(\varphi_{R,t+1}-\varphi_{M1}) + (1+\beta\,\varphi_k)\gamma_t} \\
\Leftrightarrow\; & E_t = \frac{v(1+\beta\,\varphi_k)}{\beta(\varphi_{R,t+1}-\varphi_{M1}) + (1+\beta\,\varphi_k)\gamma_t} + \sum_{i=2}^{r}\sum_{j=1}^{r} f_{i,j}\left({f'_{i,j}}^{-1}\left(\frac{-\varphi_{Mj}+\varphi_{Mi}}{\varphi_{R,t+1}-\varphi_{M1}+\Gamma}\right)\right),
\end{aligned} \tag{39}$$

where we used (38) in the last step. The first order conditions can be solved to obtain the optimal controls x_t^*, E_t^*, and $G^*_{i,j,t}$, which are independent of the states. Using E_t^* and $G^*_{i,j,t}$ one can solve for the optimal net energy input I_t^*.

$$I_t^* = E_t^* - \sum_{i=2}^{r}\sum_{j=1}^{r} f_{i,j}(G^*_{i,j,t}) = \frac{v(1+\beta\,\varphi_k)}{\beta(\varphi_{R,t+1}-\varphi_{M1}) + (1+\beta\,\varphi_k)\gamma_t} \tag{40}$$

Inserting the optimal controls into (34) and arranging terms with respect to their states yields

$$\begin{aligned}
&\varphi_k\,k_t + \boldsymbol{\varphi}_M^T\,\boldsymbol{M}_t + \varphi_{R,t}\,R_t + \varphi_t = \Big[(1+\beta\,\varphi_k)\kappa\Big]k_t + \Big[\beta\,\boldsymbol{\Phi}\boldsymbol{\varphi}_M^T - (1+\beta\,\varphi_k)\xi_0\,\boldsymbol{e}_1^T\Big]\boldsymbol{M}_t \\
&+ \Big[\beta\,\varphi_{R,t+1}\Big]R_t + \log\,x_t^* + \beta\,\varphi_k\,\log(1-x_t^*) + (1+\beta\,\varphi_k)\log A_t - (1+\beta\,\varphi_k)(\kappa+v)\log N_t \\
&+ (1+\beta\,\varphi_k)v\log I_t^* + (1+\beta\,\varphi_k)\xi_0\,M_1^{pre} + \beta\,\varphi_{M1}(E_t^* + E_t^{\text{exo}} - G^*_{i,1,t}) + \beta\,\varphi_{M2}\,G^*_{2,j,t} + ...+ \\
&(1+\beta\,\varphi_k)\gamma_t E_t^* + \beta\,\varphi_{Mr}\,G^*_{r,j,t} - \beta\,\varphi_{R,t+1}\,E_t^* + \beta\,\varphi_{t+1}.
\end{aligned} \tag{41}$$

Given the optimal controls the maximized Bellman equation is linear in all states.

Shadow prices. Coefficient matching with respect to log capital, k_t, yields

$$\varphi_k = (1+\beta\,\varphi_k)\kappa \quad\Leftrightarrow\quad \varphi_k = \frac{\kappa}{1-\beta\,\kappa}. \tag{42}$$

Inserting φ_k into equation (35) gives the optimal consumption rate $x_t^* = 1-\beta\,\kappa$.

Matching coefficients for each state from both sides of the equation leads to

$$\boldsymbol{\varphi}_M^T = -\xi_0 \, (1 + \beta \, \varphi_k) \, \boldsymbol{e}_1^T \, [\mathbf{1} - \beta \, \boldsymbol{\Phi}]^{-1}$$

Using (42) the vector of shadow prices turns to

$$\boldsymbol{\varphi}_M^T = -\xi_0 \, \frac{1}{1 - \beta \, \kappa} \, \boldsymbol{e}_1^T \, [\mathbf{1} - \beta \, \boldsymbol{\Phi}]^{-1} \tag{43}$$

Coefficient matching with respect to the resource stock yields

$$\varphi_{R,t} = \beta \, \varphi_{R,t+1} \quad \Leftrightarrow \quad \varphi_{R,t} = \beta^{-t} \varphi_{R,0} \quad \text{(Hotelling's rule)}. \tag{44}$$

The initial shadow price of the fossil resource, $\varphi_{R,0}$, depends on the whole set up of the economy, including assumptions about production and the energy sector. Given the coefficients and the optimal rate of consumption equation (41) turns to the following condition:

$$\begin{aligned} \varphi_t - \beta \, \varphi_{t+1} = \log \, x_t^* + \beta \, \varphi_k \, \log(1 - x_t^*) + (1 + \beta \, \varphi_k) \log A_t - (1 + \beta \, \varphi_k)(\kappa + v) \log N_t \\ + (1 + \beta \, \varphi_k) v \log I_t^* + (1 + \beta \, \varphi_k) \xi_0 \, M_1^{pre} + \beta \, \boldsymbol{\varphi}_M^T \, \boldsymbol{E}_t^* - \beta \, \varphi_{R,t+1} \, E_t^* \end{aligned}$$

This condition is solved by the sequence of φ_t, $t = 0, 1, \ldots$, i.e. the time-related shadow prices. The additional condition $\lim_{t \to \infty} \beta^t V(\cdot) = 0 \Rightarrow \lim_{t \to \infty} \beta^t \varphi_t = 0$ pins down the initial value φ_0.

B Proof of Proposition 1

Inserting the solutions for the shadow prices, i.e., equations (42) to (44), into (38) yields

$$G_{i,j,t}^* = {f'_{i,j}}^{-1} \left(\frac{\beta \, \xi_0 \, [(\mathbf{1} - \beta \, \boldsymbol{\Phi})^{-1}]_{1,j} - \beta \, \xi_0 \, [(\mathbf{1} - \beta \, \boldsymbol{\Phi})^{-1}]_{1,i}}{\beta \, \xi_0 \, [(\mathbf{1} - \beta \, \boldsymbol{\Phi})^{-1}]_{1,1} + (1 - \beta \, \kappa) \beta^{-t} \varphi_{R,0} + \gamma_t} \right), \tag{45}$$

where $[\cdot]_{1,1}$ denotes the first, and $[\cdot]_{1,i}$ denotes the i^{th} element of the first row of the inverted matrix in square brackets. As, by convention, costs are measured at the carbon sink, and positive only for a positive carbon transfer, we obtain that $G_{i,j,t}^* = 0$ whenever $[(\mathbf{1} - \beta \, \boldsymbol{\Phi})^{-1}]_{1,1} \leq [(\mathbf{1} - \beta \, \boldsymbol{\Phi})^{-1}]_{1,i}$.

C Proof of Proposition 2

Inserting the solutions for the shadow prices, i.e., equations (42) to (44), into (39) yields

$$E_t^* = \frac{v}{\beta\,\xi_0\,\left[(\mathbf{1}-\beta\,\mathbf{\Phi})^{-1}\right]_{1,1} + (1-\beta\,\kappa)\beta^{-t}\varphi_{R,0} + \gamma_t} + \sum_{i=2}^{r}\sum_{j=1}^{r} f_{i,j}(G_{i,j,t}^*), \tag{46}$$

where $G_{i,t}^*$ is given by equation (45).

D Proof of Proposition 3

Consider the climate-economy model from section 2 without the option of CDR, and let the variables of this model specification be denoted by a tilde.

From the first order condition (36) it follows that optimal emissions without the option of CDR are given by

$$\tilde{E}_t^* = \frac{v}{\beta\,\xi_0\,\left[(\mathbf{1}-\beta\,\mathbf{\Phi})^{-1}\right]_{1,1} + (1-\beta\,\kappa)\beta^{-t}\tilde{\varphi}_{R,0} + \gamma_t}. \tag{47}$$

The only endogenous term in equation (47) is the initial shadow price of the fossil resource stock, which is denoted by $\tilde{\varphi}_{R,0}$. In both model specifications, the size of the resource stock is the same and the entire fossil resource will be used up eventually. Therefore,

$$R_0 = \sum_{t=0}^{\infty} E_t^* = \sum_{t=0}^{\infty} \tilde{E}_t^*.$$

Using equations (46) and (47), and rearranging leads to

$$\sum_{t=0}^{\infty}\sum_{i=2}^{r}\sum_{j=1}^{r} f_{i,j}(G_{i,j,t}^*) = \sum_{t=0}^{\infty}\left(\frac{v}{\beta\,\xi_0\,\left[(\mathbf{1}-\beta\,\mathbf{\Phi})^{-1}\right]_{1,1} + (1-\beta\,\kappa)\beta^{-t}\tilde{\varphi}_{R,0} + \gamma_t} - \frac{v}{\beta\,\xi_0\,\left[(\mathbf{1}-\beta\,\mathbf{\Phi})^{-1}\right]_{1,1} + (1-\beta\,\kappa)\beta^{-t}\varphi_{R,0} + \gamma_t}\right).$$

If there exists at least one point in time where $\sum_{i=2}^{r}\sum_{j=1}^{r} f_{i,j}(G_{i,j,t}^*) > 0$, the left term of the equation is positive, and thus $\tilde{\varphi}_{R,0} < \varphi_{R,0}$. From this it directly follows that $I_t^* - \tilde{I}_t^* < 0$.

Comparing net emissions with and without the option of CDR yields

$$\Delta E_t^{net^*} \equiv E_t^{net^*} - \tilde{E}_t^{net^*} = I_t^* - \tilde{I}_t^* + \sum_{i=2}^{r}\sum_{j=1}^{r}\left(f_{i,j}(G_{i,j,t}^*) - G_{i,j,t}^*\right) < 0,$$

as $\tilde{I}_t^* > I_t^*$ and $f_{i,j}(G_{i,j,t}) \leq G_{i,j,t}^*$.

E The social cost of carbon in Reservoir i, (SCC_{Mi})

The SCC of carbon in reservoir i is the negative of the shadow price of carbon reservoir i, expressed in money-measured consumption units,

$$SCC_{Mi} = -(1-\beta\,\kappa)Y_t^{net}\,\varphi_{Mi} = Y_t^{net}\,\xi_0\,\left[(\mathbf{1}-\beta\,\mathbf{\Phi})^{-1}\right]_{1,i},$$

where again $[\cdot]_{1,i}$ denotes the i^{th} element of the first row of the inverted matrix in square brackets.

F Renewable energy

Total energy is given by equation (17), where we let green energy $E_{g,t}$ evolve exogeneously with an upper bound $\bar{E}_{g,t}$. Exogenous technological progress in the fossil industry is determined by $A^s_{f,t}$ and the carbon content is given by $E_{f,t}$.

Maximizing the right side of the Bellman equation over CDR from reservoir j with storage in reservoir i, $G_{i,j,t}$, yields

$$-v(1+\beta\,\varphi_k)\,\frac{f'_{i,j}(G_{i,j,t})}{I_t} = \beta(\varphi_{Mj}-\varphi_{Mi}). \tag{48}$$

The first order condition for fossil fuel use delivers

$$(1+\beta\,\varphi_k)\,\left(\frac{v}{I_t}-\gamma_t\right)\left(aA^s_{f,t}E^s_{f,t}+(1-a)E^s_{g,t}\right)^{\frac{1}{s}-1}aA^s_{f,t}E^{s-1}_{f,t} = \beta(\varphi_{R,t+1}-\varphi_{M1}). \tag{49}$$

Inserting equations (48) and (17) into (49) leads to

$$\left(-\frac{\beta(\varphi_{Mj}-\varphi_{Mi})}{f'_{i,j}(G_{i,j,t})}-(1+\beta\,\varphi_k)\gamma_t\right)aA^s_{f,t}\left(\frac{E_{f,t}}{E_t}\right)^{s-1} = \beta(\varphi_{R,t+1}-\varphi_{M1})$$

Solving for $G_{i,j,t}$ we obtain

$$G^*_{i,j,t} = {f'_{i,j}}^{-1}\left(\frac{-\beta(\varphi_{Mj}-\varphi_{Mi})}{\frac{\beta(\varphi_{R,t+1}-\varphi_{M1})}{aA^s_{f,t}}\left(\frac{E_{f,t}}{E_t}\right)^{1-s}+(1+\beta\,\varphi_k)\gamma_t}\right). \tag{50}$$

Plugging in the solutions for the shadow prices we get equation (18).

G Calibration

G.1 Energy costs

Energy producing firms solve the following maximization problem,

$$\max_{E_g, E_f} \quad Z(a\, E_f^s + (1-a) E_g^s)^{\frac{1}{s}} - p_f\, E_f - p_g\, E_g,$$

where Z denotes the value of a unit of energy. The first order conditions are given by

$$Z\, a\, E_f^{s-1} (a\, E_f^s + (1-a) E_g^s)^{\frac{1-s}{s}} = p_f \tag{51}$$

$$Z\, (1-a)\, E_g^{s-1} (a\, E_f^s + (1-a) E_g^s)^{\frac{1-s}{s}} = p_g \tag{52}$$

Solving equation (51) for a leads to

$$a = \frac{p_f\, E_f^{1-s}}{Z\, E_f^{s-1} (a\, E_f^s + (1-a) E_g^s)^{\frac{1-s}{s}}} \tag{53}$$

Rewriting of equations (51) and (52) yields

$$Z\, a\, (a\, E_f^s + (1-a) E_g^s)^{\frac{1-s}{s}} = p_f\, E_f^{1-s} \tag{54}$$

$$Z\, (1-a)\, (a\, E_f^s + (1-a) E_g^s)^{\frac{1-s}{s}} = p_g\, E_g^{1-s} \tag{55}$$

Adding up equations (51) and (52) we get

$$Z\, E_f^{s-1} (a\, E_f^s + (1-a) E_g^s)^{\frac{1-s}{s}} = p_f\, E_f^{1-s} + p_g\, E_g^{1-s} \tag{56}$$

Thus, we can write euqtion (53) as

$$a = \frac{p_f\, E_f^{1-s}}{p_f\, E_f^{1-s} + p_g\, E_g^{1-s}} \tag{57}$$

To calibrate the parameter a we use data on energy production by different sources from International Energy Agency (2024), listed in the Table below.

Table 7: Energy production in 2020 (average) by energy source (measured in EJ).

Oil	Coal	Natural gas	Nuclear	Hydro	Wind & solar	Biofuel & waste
184.69	164.51	140.45	29.86	15.46	15.30	52.57

We collected price data for 2020 (average from 2018 to 2022) from the World Bank (2023) and International Renewable Energy Agency (2024). To isolate the production costs for oil, coal and gas, we use data on resource rents from the World Bank (2024).

Based on this data we calculate the production weighted cost parameter $\gamma = 0.011\%$ of global GDP/EJ and the CES share parameter $a = 0.38$.

Table 8: Energy prices in 2020 by source in USD.

Oil	Coal	Natural gas	Nuclear	Hydro	Wind (on/off)	Solar	Biofuel
67.84	134.70	10.03	69.00	0.04	0.11/0.20	0.45	0.08
/bbl	/mt	/mmbtu	/mwh	/kwh	/kwh	/kwh	/kwh

G.2 Climate change damages

Golosov et al. (2014) calibrate the climate damage parameter, ξ, in (7), by using the climate change damage estimate provided by Nordhaus (2007) which is a function of temperature. For their calibration, Golosov et al. (2014) rely on the equilibrium climate sensitivity (ESC) to link atmospheric carbon concentration, M_1, to temperature increase:

$$T^{AT} = T^{AT}(M_1) = ESC * \left(\frac{ln(M_1/M_{1,pre})}{ln(2)} \right). \tag{58}$$

However, the climate change damages are primarily determined by the actual temperature, which rises more slowly than specified by the ESC, but is also influenced by non-CO_2 forcing. This is how the climate damages in DICE-type IAMs are usually integrated into the economic optimization problem. The rate at which the temperature increases is determined by the transient climate response (TCR). Formally, "ECS is the magnitude of the long-term GSAT [global mean surface air temperature] increase in response to a doubling of atmospheric CO_2 concentration after the planetary energy budget is balanced, though leaving out feedbacks associated with ice sheets; whereas the TCR is the magnitude of GSAT increase at year 70 when CO_2 concentration is doubled in a 1% yr^{-1} increase scenario. [...] TCR is always smaller than ECS because ocean heat uptake acts to reduce the rate of surface warming(Forster et al. 2021, p. 992)." Accordingly, the ESC would not be affected by carbon sink saturation effects as these "only" imply that the ESC is achieved at later point in time.

Using the functional form (7) and calibrating it, using the ESC, implies that damages for low (high) atmospheric carbon concentration are overestimated (underestimated). Figure 7 shows the implication of this calibration strategy.

The left panel shows the loss in output as a function of increasing atmospheric carbon concentration (M_1) based the calibration of Golosov et al. (2014), using Nordhaus (2007) impact estimate. The solid blue line is based on the ESC, using the central estimate from the recent IPCC AR6 report (Forster et al. 2021), i.e., ESC=3°, the dashed, blue lines is based on the ESC, using the central estimate from the CDICE calibration of Folini et al. (2025), i.e., ESC=3.25°, and the black line is based on carbon concentration only,

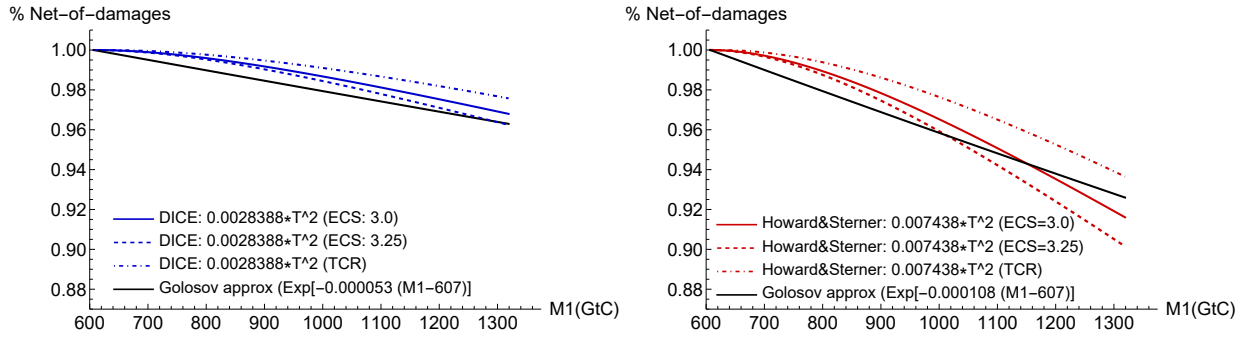

Figure 7: Representation of climate change damages, left panel based on the parameter value obtained from Golosov et al. (2014) and right panel calibrated to the damage estimate of Howard and Sterner (2017), using the again the Golosov et al. (2014) approximation strategy.

using the parameter from Golosov et al. (2014). The blue, dot-dashed line shows the loss in output resulting from the temperature as it would evolve in our model, i.e using the energy-balance model provided by Folini et al. (2025) and accounting for non-CO_2-forcing. Note that the latter is time-dependent,i.e., the length of time that the carbon cycle is exposed to the anthropogenic disturbance resulting from carbon emissions. We have followed here the CMIP protocol as explained above, i.e., increasing atmospheric carbon concentration each year by 1 percent. The carbon cycle and energy balance model calibration by Folini et al. (2025) result in a TCR of 2.59°C and 1.99°C with and without exogenous forcing. The central value in the combined assessment, presented in IPCC AR6, is 1.8°C with the likely range being 1.4°C to 2.2°C and the very likely range being 1.2°C to 2.4°C (Forster et al. 2021). Hence, even with a temperature response at the upper range, as resulting from the CDCICE carbon-cycle-climate model, the Golosov et al. damage function calibration overestimates damages in the domain from 800 GtC (assumed as starting conditions) and 1300 GtC (which is above peak atmospheric carbon concentration in the BAU scenario) compared to the DICE damage function.

The right panel shows the loss in output as a function of increasing atmospheric carbon concentration based on our calibration, using the Howard and Sterner (2017) impact estimate for non-catastrophic climate change. For consistency, we follow the calibration strategy by using the loss in output under the ESC-temperature response (with ESC=3°) for a doubling of CO_2 concentration, using the Nordhaus damage function with the parameter obtained from Howard and Sterner (2017). The solid red line is based on the ESC, using the central estimate from the recent IPCC AR6 report (Forster et al. 2021), i.e., ESC=3°, the dashed, blue lines is based on the ESC, using the central estimate from the CDICE calibration of Folini et al. (2025), i.e., ESC=3.25°, and the black line is based on carbon concentration only, using the parameter $\xi_{hs} = 10.8 \times 10^{-5}$. The red, dot-dashed line shows the loss in output resulting from the temperature as it would evolve in our model, i.e using the energy-balance model provided by Folini

et al. (2025) and accounting for non-CO_2-forcing, with the damage parameter obtained from Howard and Sterner (2017). Again, the damage function calibration using (7) and following the calibration strategy of Golosov et al. (2014), overestimates damages in the domain from 800 GtC (assumed as starting conditions) and 1300 GtC (which is above peak atmospheric carbon concentration in the BAU scenario) as they would materialize in our model.

However, this only holds true in levels and in particular the stronger curved damage function in the right-panel indicates that our representation overestimates and underestimates marginal damages for low and high atmospheric carbon concentrations, in the considered domain. This is clearly a limitation of our model to keep in mind when interpretation the results.

To assess the severity of this limitation, we include as alternative specification, a damage function which is quadratic in the ESC-temperature response, i.e.,

$$D_t^{alt}(M_{1,t}) = 1 - \theta * T_t(M_{1,t})^2 = 1 - \theta * ESC * \left(\frac{ln(M_1/M_{1,pre})}{ln(2)}\right)^2. \tag{59}$$

The results are discussed in Figure 10 in Appendix H.

G.3 CDR cost

CDR	**Source**	**Costs ($/tC)**		**Potential (GtC/10yr)**	
		Min	**Max**	**Min**	**Max**
OIF	Babiker et al. (2022)	183.35	1,833.50	2.73	8.18
	NASEM (2021)	91.68	183.35	0.27	2.73
	Emerson et al. (2024)	77.01	17,201.90	2.73	8.18
OAE	Babiker et al. (2022)	146.68	953.42	10.00	100.00
	NASEM (2021)	366.70	550.05	10.00	100.00
	Kowalczyk et al. (2024)	476.71	1,081.77	10.00	100.00
DACCS	Babiker et al. (2022)	366.70	1,100.10	1.36	100.00
	NASEM (2021)	308.03	1,415.46	1.36	100.00
	Young et al. (2023)	366.70	2,200.20	1.36	100.00

Table 9: Cost and carbon removal potential estimates from the literature. NASEM (2021) abbreviates the source National Academies of Sciences, Engineering, and Medicine (2021).

Table 10 lists the results of the idealized carbon cycle experiment for the different calibrations of the carbon cycle to determine the removal efficiency.

	OIF	OAE	DACCS
MM	0.86	0.98	1.00
LS	0.85	0.98	1.00
HS	0.86	0.98	1.00
Average	0.86	0.98	1.00

Table 10: Cost correction factors for cost estimates in the literature for the different CDR methods derived based on their carbon removal pathway.

G.4 CCS cost

CCS	Source	Costs ($/tC)		Potential (GtC/10yr)	
		Min	Max	Min	Max
	IPCC (2005)	51.34	333.70	5.00	100.00
	Rubin et al. (2015)	139.35	524.38	5.00	100.00
	Bennæs et al. (2023)	198.86	438.46	5.00	100.00

Table 11: Cost and CCS potential estimates from the literature. IPCC (2005) abbreviates the source Intergovernmental Panel on Climate Change (2005).

Note that some studies presented in Table 11 do not provide estimates of removal potential. In this case we relied on the removal range from the other studies.

H Additional results

Table 12 shows annual deployment levels of CDR and CCS for the different scenarios under the baseline climate damage specification.

Figure 8 supplements Figure 3 in the main text, showing the net carbon benefit for the different CDR methods, resulting from the SCC and the carbon dynamics multipliers, whereas the latter adjust the SCC to the different storage sides. The presented values show the mean across the different policies (i.e. with or without CDR and CCS). The net carbon benefit for DACCS is shown for the case of permanent storage.

Figure 9 supplements Figure 3 in the main text, showing the long-term evolution of ocean carbon storage. The figure is based on Figure 9 in Kheshgi and Archer (2004), which is also shown as Figure 6.2 in Intergovernmental Panel on Climate Change (2005). The figure shows for an emission path of cumulative 5000 GtC (Panel a shows the emissions rate and Panel b shows the cumulative emissions), the evolution of atmospheric carbon concentration, starting at preindustrial level, using the mean carbon cycle calibration obtained from Folini et al. (2025) (Panel c). The displayed cases include 100% of emissions released to the atmosphere, 100% of emissions injected into the ocean (no emissions to

year		2030		2050		2100		2200	
		Average	Std	Average	Std	Average	Std	Average	Std
in GtC/year									
individual	DACCS	0.00	0.00	0.24	0.37	2.68	2.19	8.64	1.47
CDR	OAE	0.00	0.00	0.28	0.47	2.88	2.77	8.42	2.36
	OIF	0.06	0.06	0.08	0.08	0.13	0.13	0.35	0.35
only CCS	CCS	1.04	0.44	2.52	1.05	5.45	1.12	1.45	0.22
combined	total CDR	0.06	0.06	0.48	0.46	4.93	3.00	8.20	2.84
CDR	DACCS	0.00	0.00	0.20	0.30	2.40	1.93	4.94	2.11
	OAE	0.00	0.00	0.21	0.35	2.42	2.29	3.16	1.90
	OIF	0.06	0.06	0.07	0.07	0.11	0.11	0.11	0.18
combined	total CDR	0.06	0.06	0.26	0.25	3.80	2.17	3.66	2.56
CDR&CCS	DACCS	0.00	0.00	0.10	0.17	1.87	1.45	2.10	1.91
	OAE	0.00	0.00	0.09	0.17	1.81	1.61	1.37	1.66
	OIF	0.06	0.06	0.07	0.08	0.11	0.12	0.19	0.34
	CCS	0.86	0.37	2.21	0.92	4.62	1.45	1.14	0.46

Table 12: Optimal levels of CDR and CCS deployment for the baseline climate damage specification, showing the results for deployment of individual CDR methods, of individual CCS deployment, combined CDR deployment, and combined CDR deployment with CCS.

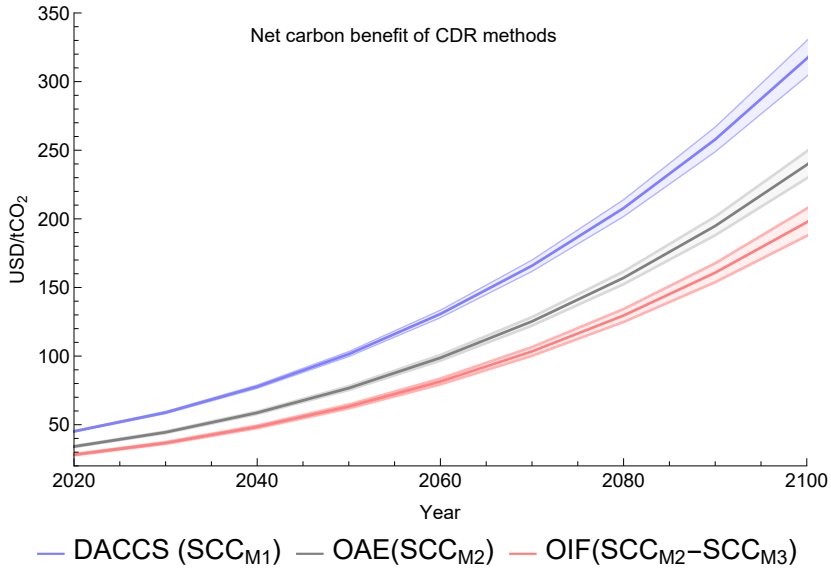

Figure 8: Net carbon benefit for the different CDR methods, showing the mean and the shaded area ±SD.

the atmosphere), 100 percent emissions released to the atmosphere until the year 2050, followed by 50% of emissions released to the atmosphere and 50% of emissions injected into the ocean, 100% emissions released into the atmosphere until the year 2050, followed by 50% of emissions released to the atmosphere while the other 50% are mitigated, and no emissions at all.

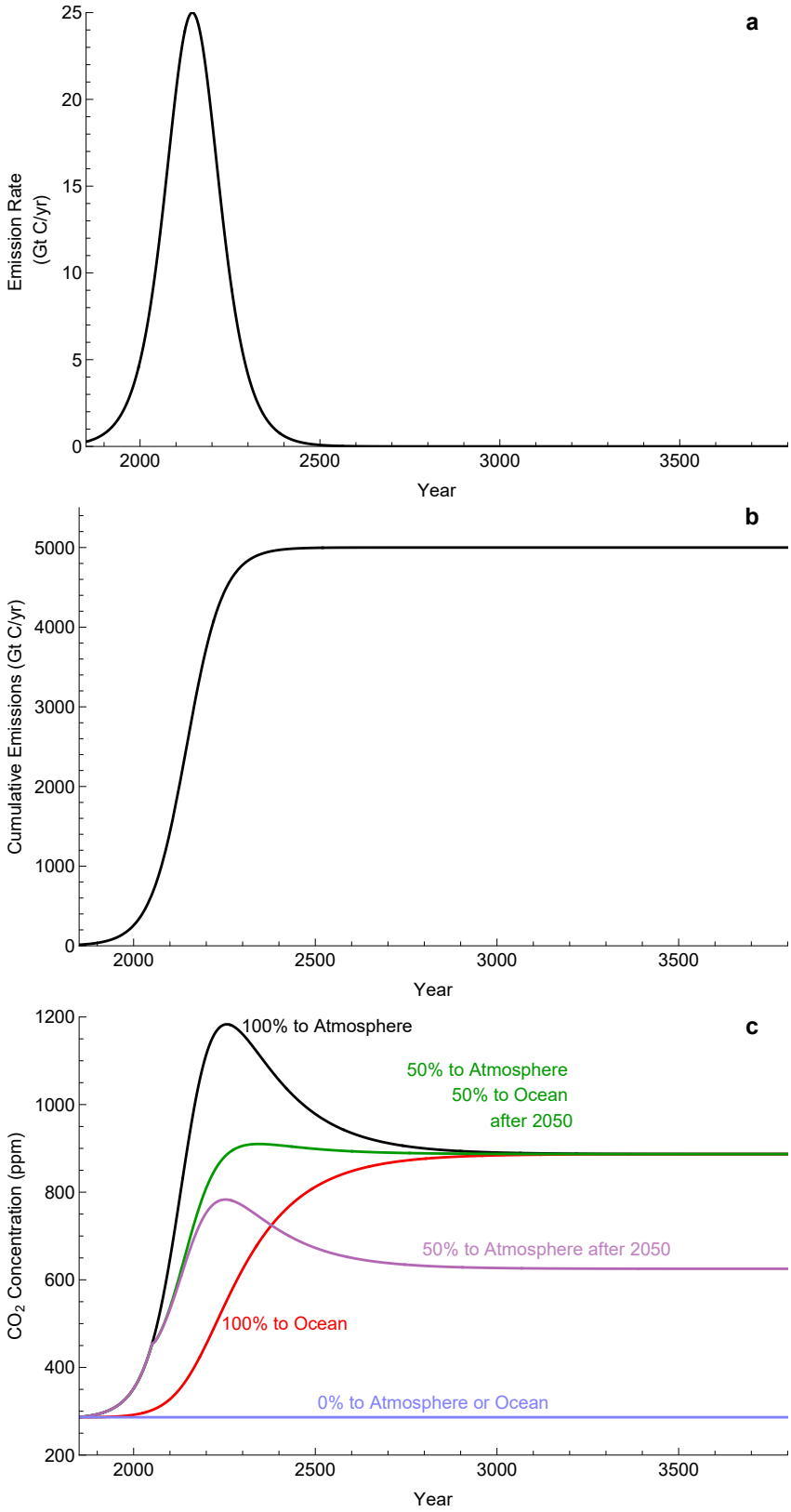

Figure 9: Simulated atmospheric CO_2 resulting from CO_2 release to the atmosphere or injection into the ocean.

Figure 10 shows the implications of our damage function (7) by comparing optimal climate policies with combined CCS under this representation of climate damages to a representation which is quadratic in the equilibrium temperature response, i.e., (G.2). As explained Section G.2, our damage function overestimates damages, in particular for low concentration, however, missed the steepness of a quadratic damage function in temperature. Our figure indicates that this results in only a small deviation, in particular after 2100 when atmospheric carbon concentration becomes lower again. Nevertheless, we consider the results obtained under our assumption therefore a good approximation for results obtained under a steeper damage function, at least for the policy relevant domain until the year 2100.

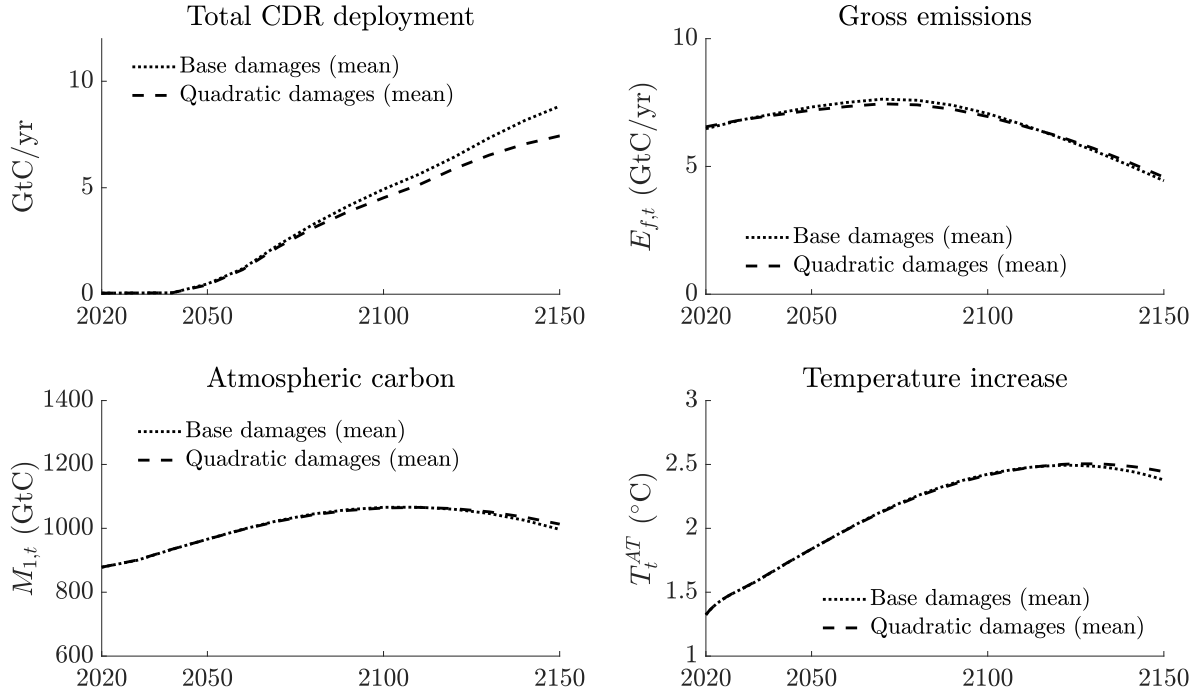

Figure 10: Optimal climate policies with combined deployment of CDR methods for baseline damage impact estimate, either represented as exponential function of atmospheric carbon concentration (base damages), (7), or as quadratic function of the equilibrium temperature response (quadratic damages), (G.2).

Figure 11 shows the implications of the two alternative carbon cycle calibrations, 'MESMO' and 'LOVECLIM', based on the parameters in Table 2 in the main text. These two calibrations can be interpreted as scientifically plausible, yet extreme, carbon cycle behaviors. To achieve this behavior, not only the parameter of the transition matrix are adjusted but also the implicit equilibrium values of the non-atmospheric carbon boxes. The three carbon cycle calibrations have equilibrium fractions of 26, 23, and 34 percent of cumulative emissions remaining in the atmosphere for the average sink calibration (CDICE), the fast sink calibration (LOVECLIM), and the slow sink calibration

(MESMO), respectively. The equilibrium fraction is increasing in the amount of cumulative emissions (Sarmiento and Gruber 2006). Given the initial carbon stocks in our analysis (i.e., the cumulative past emissions) and the fossil resource stock (i.e., the possible future emissions), we have a potential upper anthropogenic perturbation of about 1600 GtC. Sarmiento and Gruber (2006) report an equilibrium fraction of about 21 percent being in the atmosphere for an anthropogenic pertubation of 1800 GtC (and equilibrium refers here to a short-term equilibrium, i.e., on millenial time-scales before long-term processes like the sentimentary buffer become relevant). Accordingly, one could argue that the results displayed under the 'LOVECLIM' calibration should be considered as likely as the results under 'CDICE'. Still, 'MESMO' also provides relevant insights since it might show the implications of an unexpected strong weakening of the ocean carbon sink (Liu et al. 2023). Figure 11 shows the implications of the different carbon cycle calibrations for total CDR deployment, the individual methods, and the implications for gross emissions and temperature increase.

First, we can notice that slower (faster) carbon uptake by sinks, results in more (less) CDR deployment, compared to the average calibration. With slower (faster) carbon uptake by sinks, atmospheric carbon concentration and temperature increases (decreases), the SCC increase (decrease) and in turn the benefits of CDR increase (decrease), compared to the average calibration. Comparing the results from the calibration based on 'MESMO' with 'LOVECLIM' shows that the faster sink in 'LOVECLIM' does part of the job of CDR. However, there is a second effect. The calibration of 'MESMO' implies that the upper ocean becomes a stronger bottleneck in transfering carbon into the deep ocean, accordingly, the increase in OIF and in OAE compared to the 'CDICE' calibration is stronger than this is the case for DACCS. Hence, in a scenario with already weakened ocean sink, the ocean-based CDR approaches become relatively more efficient.

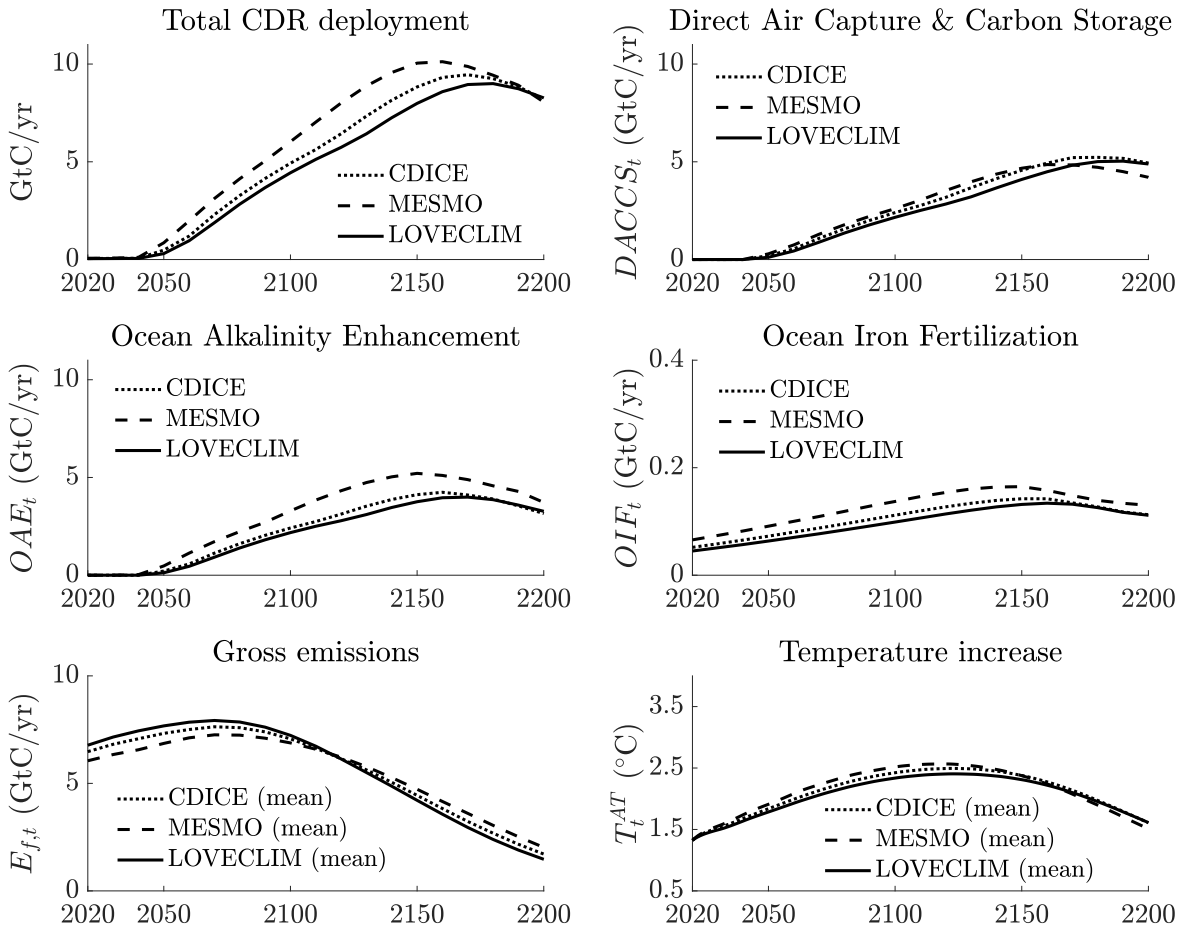

Figure 11: The graphs show the differences in CDR deployment levels for LOVECLIM and MESMO (in comparison to CDICE). The bottom left (right) graph shows gross emissions (temperature increase) for the different carbon cycle calibrations.

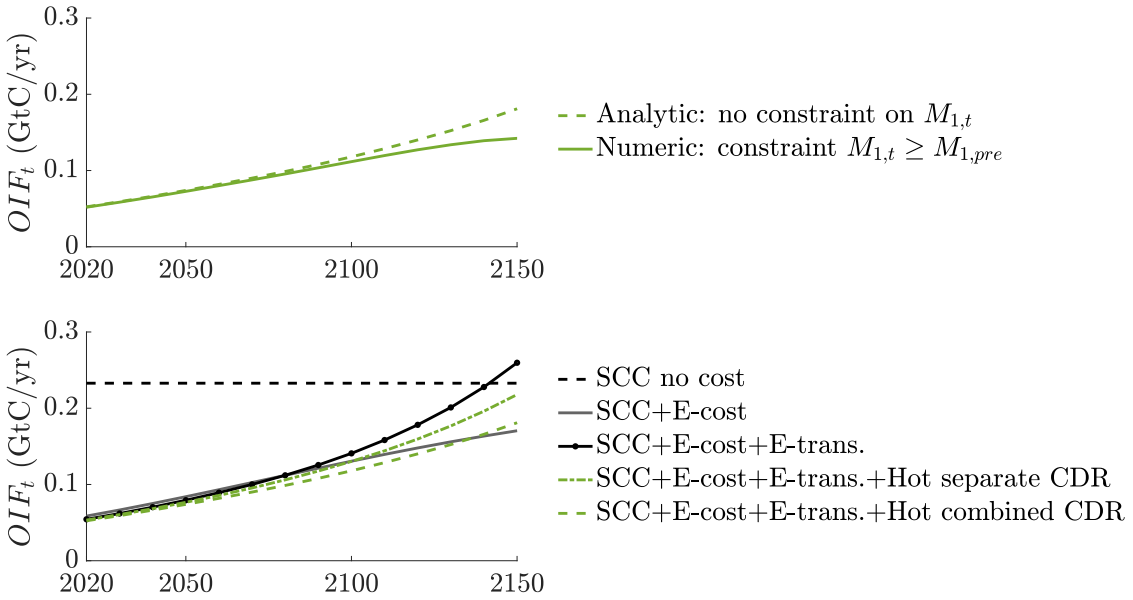

Figure 12: The upper graph show optimal OIF deployment based on the analytical formula derived in equation (18) and the numerical outcome. The lower graph shows the different contributions to optimal OIF deployment for the combined and individual case. The terms in the legend refer to the definitions in equation (18).

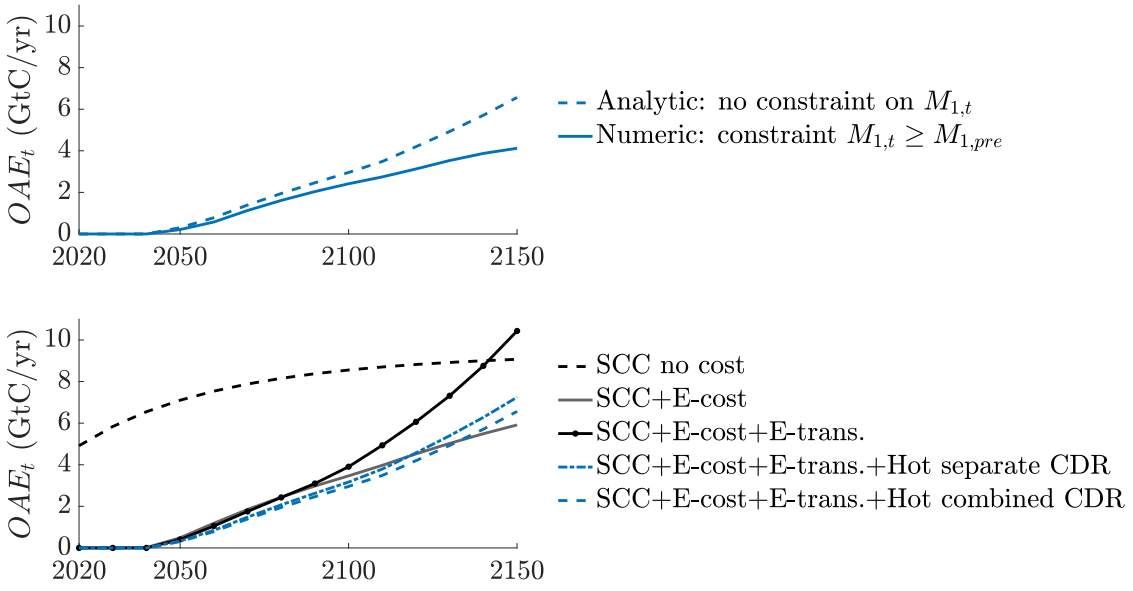

Figure 13: The upper graph show optimal OAE deployment based on the analytical formula derived in equation (18) and the numerical outcome. The lower graph shows the different contributions to optimal OAE deployment for the combined and individual case. The terms in the legend refer to the definitions in equation (18).

Damages	Policy	2100		2200	
		Mean	pessimistic/ optimistic	Mean	pessimistic/ optimistic
Cumulative CDR by ... (in GtC)					
Baseline	woCDRwoCCS	0		0	
	wCDRwoCCS	165	2 / 444	980	245 / 1815
	woCDRwCCS	0		0	
	wCDRwCCS	126	2 / 284	120	120 / 1231
High	woCDRwoCCS	0		0	
	wCDRwoCCS	351	70 / 737	1283	540 / 2219
	woCDRwCCS	0		0	
	wCDRwCCS	262	41 / 564	644	217 / 1206
Cumulative CCS by ... (in GtC)					
Baseline	woCDRwoCCS	0		0	
	wCDRwoCCS	0		0	
	woCDRwCCS	276	157 / 413	662	491 / 849
	wCDRwCCS	237	140 / 402	572	279 / 824
High	woCDRwoCCS	0		0	
	wCDRwoCCS	0		0	
	woCDRwCCS	425	341 / 528	889	737 / 1038
	wCDRwCCS	406	324 / 546	776	506 / 1067
Share of energy consumption for CDR and CCS (in percent)					
Baseline	woCDRwoCCS	0		0	
	wCDRwoCCS	5	0 / 9	5	0 / 12
	woCDRwCCS	6	6 / 5	0	0 / 1
	wCDRwCCS	8	5 / 10	3	0 / 9
High	woCDRwoCCS	0		0	
	wCDRwoCCS	15	10 / 16	4	0 / 15
	woCDRwCCS	8	10 / 5	1	0 / 1
	wCDRwCCS	16	17 / 19	1	0 / 2

Table 13: Cumulative CDR and CCS emissions by the year 2100 and 2200 for the different policies and anual energy share for these methods in the year 2100 and 2200. the The policies differ whether they include (with, 'w') or exclude (without, 'wo') CDR and CCS. Only those climate policies with CDR and CCS include various scenarios, accordingly we display here also the results for the scenario with the most pessimistic and optimistic development of CDR and CCS costs.